Inorganic Chemistry

Article

pubs.acs.org/IC

Theoretical Insights into the Ferromagnetic Coupling in Oxalato-Bridged Chromium(III)-Cobalt(II) and Chromium(III)-Manganese(II) Dinuclear Complexes with Aromatic Diimine Ligands

Julia Vallejo,[†] Isabel Castro,*[,†] Mariadel Déniz,[‡] Catalina Ruiz-Pérez,[‡] Francesc Lloret,[†] Miguel Julve,[†] Rafael Ruiz-García,[†,§] and Joan Cano*[,†,§]

[†]Instituto de Ciencia Molecular (ICMol) and [§]Fundació General de la Universitat de València (FGUV), Universitat de València, E-46980 Paterna, València, Spain

[‡]Laboratorio de Rayos X y Materiales Moleculares, Departamento de Física Fundamental II, Facultad de Física, Universidad de la Laguna, E-38204 La Laguna, Tenerife, Spain

Supporting Information

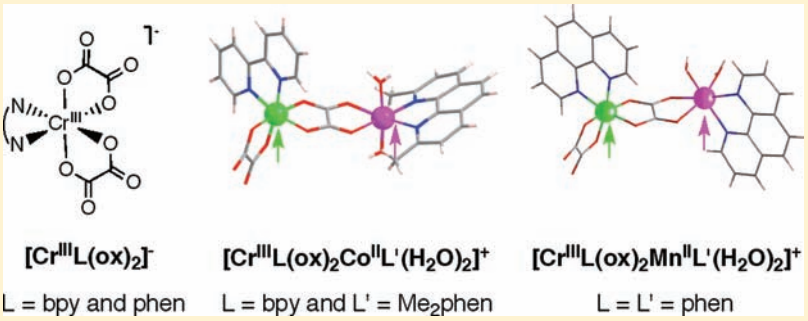

ABSTRACT: Two novel heterobimetallic complexes of formula $[Cr(bpy)(ox)_2Co(Me_2phen)(H_2O)_2][Cr(bpy)(ox)_2]\cdot 4H_2O$ (**1**) and $[Cr(phen)(ox)_2Mn(phen)(H_2O)_2][Cr(phen)(ox)_2]\cdot H_2O$ (**2**) (bpy = 2,2′-bipyridine, phen = 1,10-phenanthroline, and Me_2phen = 2,9-dimethyl-1,10-phenanthroline) have been obtained through the "complex-as-ligand/complex-as-metal" strategy by using $Ph_4P[CrL(ox)_2]\cdot H_2O$ (L = bpy and phen) and $[ML'(H_2O)_4](NO_3)_2$ (M = Co and Mn; L′ = phen and Me_2phen) as precursors. The X-ray crystal structures of **1** and **2** consist of bis(oxalato)chromate(III) mononuclear anions, $[Cr^{III}L(ox)_2]^-$, and oxalato-bridged chromium(III)-cobalt(II) and chromium(III)-manganese(II) dinuclear cations, $[Cr^{III}L(ox)(\mu\text{-ox})M^{II}L'(H_2O)_2]^+$ [M = Co, L = bpy, and L′ = Me_2phen (**1**); M = Mn and L = L′ = phen (**2**)]. These oxalato-bridged $Cr^{III}M^{II}$ dinuclear cationic entities of **1** and **2** result from the coordination of a $[Cr^{III}L(ox)_2]^-$ unit through one of its two oxalato groups toward a $[M^{II}L'(H_2O)_2]^{2+}$ moiety with either a *trans*- (M = Co) or a *cis*-diaqua (M = Mn) configuration. The two distinct Cr^{III} ions in **1** and **2** adopt a similar trigonally compressed octahedral geometry, while the high-spin M^{II} ions exhibit an axially (M = Co) or trigonally compressed (M = Mn) octahedral geometry in **1** and **2**, respectively. Variable temperature (2.0−300 K) magnetic susceptibility and variable-field (0−5.0 T) magnetization measurements for **1** and **2** reveal the presence of weak intramolecular ferromagnetic interactions between the Cr^{III} ($S_{Cr} = 3/2$) ion and the high-spin Co^{II} ($S_{Co} = 3/2$) or Mn^{II} ($S_{Mn} = 5/2$) ions across the oxalato bridge within the $Cr^{III}M^{II}$ dinuclear cationic entities (M = Co and Mn) [J = +2.2 (**1**) and +1.2 cm^{-1} (**2**); $\mathbf{H} = -J\,\mathbf{S}_{Cr}\cdot\mathbf{S}_M$]. Density functional electronic structure calculations for **1** and **2** support the occurrence of $S = 3$ $Cr^{III}Co^{II}$ and $S = 4$ $Cr^{III}Mn^{II}$ ground spin states, respectively. A simple molecular orbital analysis of the electron exchange mechanism suggests a subtle competition between individual ferro- and antiferromagnetic contributions through the σ- and/or π-type pathways of the oxalato bridge, mainly involving the $d_{yz}(Cr)/d_{xy}(M)$, $d_{xz}(Cr)/d_{xy}(M)$, $d_{x^2-y^2}(Cr)/d_{xy}(M)$, $d_{yz}(Cr)/d_{xz}(M)$, and $d_{xz}(Cr)/d_{yz}(M)$ pairs of orthogonal magnetic orbitals and the $d_{x^2-y^2}(Cr)/d_{x^2-y^2}(M)$, $d_{xz}(Cr)/d_{xz}(M)$, and $d_{yz}(Cr)/d_{yz}(M)$ pairs of nonorthogonal magnetic orbitals, which would be ultimately responsible for the relative magnitude of the overall ferromagnetic coupling in **1** and **2**.

INTRODUCTION

Multimetallic coordination compounds of variable dimensionality are of great interest because of their attractive physical properties, such as ferro- and ferrimagnetism, porosity, chirality, multiferroism, and conductivity.[1] Besides their interest as models for the fundamental research on electron exchange phenomena between different metal centers through extended bridges,[1a] this class of heterobimetallic complexes could be also of great importance because of their future technological applications in substitution of traditional magnets based on mixed metal alloys and oxides.[1b] So, it is well-known that some paramagnetic transition metal complexes with suitably designed ligands can be used as molecular precursors against other metal

Received: December 23, 2011
Published: February 22, 2012

   dx.doi.org/10.1021/ic202755z | *Inorg. Chem.* 2012, 51, 3289−3301

ions to obtain heterobimetallic coordination compounds that order ferro- or ferrimagnetically below a critical temperature (T_c).[2−4] Relevant examples of this class of molecule-based magnets include heterobimetallic cyanides (Prussian Blue analogues),[2] oxalates and dithiooxalates,[3] as well as oxamates and oxamidates,[4] with T_c values reaching up to room temperature in the former case. More recently, coordination chemists have successfully used this molecular-programmed self-assembly mixed-metal approach to obtain mutifunctional molecular materials, such as porous magnets,[5] chiral magnets,[6] spin-crossover magnets,[7] photo- or piezo-active magnets,[8] multiferroics,[9] and protonic or electronic magnetic conductors.[10] They combine the magnetic and porous properties of the anionic heterobimetallic open-framework with the additional chiral, magnetic, dipolar, optical, redox, and conducting properties of the countercation.[5−10]

Oxalato-bridged heterobimetallic compounds, reaching from discrete zero-dimensional (0D)[11] to extended one- (1D),[8f,12] two- (2D),[6b,c,7a,8c−e,10a,b,13] and three-dimensional (3D),[7b,10c,14] were obtained when using the anionic tris(oxalato)chromate(III) mononuclear complex as building block because of its potential coordination capabilities through the *cis* carbonyl-oxygen atoms of the oxalato groups. In each case, the $[Cr^{III}(ox)_3]^{3-}$ complex acts as mono- (0D), bis- (1D), and tris- (bidentate) (2D and 3D) metalloligand toward divalent middle and late 3d metal ions, from manganese(II) to copper(II), depending on the choice of the countercation (templating agent). This family of multidimensional molecule-based magnetic materials includes some examples of single chain magnets (SCMs) exhibiting a slow relaxation of the magnetization,[12b,c] as well as open-framework magnets (OFMs) possessing a long-range magnetic ordering.[13,14] Whatever the dimensionality is, the variety of interesting magnetic behaviors exhibited by this class of mixed first-row transition metal bimetallic oxalates ultimately depends on the nature and magnitude of the intramolecular magnetic interaction through the oxalato bridge and the local magnetic anisotropy of the individual metal centers as well.

All these oxalato-bridged *n*D $M^{II}Cr^{III}$ compounds (n = 1−3) invariably behave as ferromagnets, independently of the nature of the M^{II} ion (M = Mn, Fe, Co, Ni, and Cu).[11−14] In fact, Okawa and co-workers have found a correlation between the T_c values in the seminal series of bimetallic oxalate 2D ferromagnets of general formula n-$Bu_4N[M^{II}Cr^{III}(ox)_3]$ (n-Bu_4N^+ = tetra-*n*-butylammonium cation and M = Mn, Fe, Co, Ni, and Cu)[13a,b] and the relative magnitude of the ferromagnetic coupling in an analogous series of oxalato-bridged $M^{II}Cr^{III}$ dinuclear complexes (M = Mn, Fe, Co, Ni, and Cu), expressed by the magnetic coupling parameter (J) in the spin Hamiltonian $\mathbf{H} = -J\,\mathbf{S_M}\cdot\mathbf{S_{Cr}}$.[15] At that time, the observed ferromagnetic coupling ($J > 0$) between the Cr^{III} and the M^{II} ions across the oxalato bridge was considered atypical. In general, orbital symmetry considerations dictate that the magnetic coupling between the octahedral Cr^{III} and M^{II} ions (M = Ni and Cu) would be ferromagnetic because of the orthogonal nature of the interacting magnetic orbitals, that is, the t_{2g} orbitals from the $3d^3$ Cr^{III} ion and the e_g orbitals from the high-spin $3d^n$ M^{II} ions [M = Ni (n = 8) and Cu (n = 9)].[16] On the contrary, an antiferromagnetic coupling ($J < 0$) is expected between the Cr^{III} and M^{II} ions (M = Mn, Fe, and Co) because of the nonorthogonal nature of some of the involved magnetic orbitals, that is, the t_{2g} orbitals from both the $3d^3$ Cr^{III} and the high-spin $3d^n$ M^{II} ions [M = Mn (n = 5), Fe (n = 4), and Co (n = 7)].[4b]

Our strategy in this field consists of using aromatic diimine-containing bis(oxalato)chromate(III) mononuclear complexes as metalloligands toward other coordinatively unsaturated complexes of divalent 3d metal ions, from manganese(II) to copper(II), to preclude the formation of polymeric oxalato-bridged heteropolymetallic species.[17] Using this so-called "complex-as-ligand/complex-as-metal" approach, a limited number of discrete oxalato-bridged heteropolymetallic species with nuclearities ranging from di-,[18] to tri-,[19] and tetranuclear,[20] have been prepared following the pioneering Andruh work. In this context, we recently showed that heteroleptic ferromagnetically coupled, trinuclear chromium(III)-cobalt(II) complexes, $\{[Cr^{III}L(ox)_2]_2Co^{II}L'\}$, can be rationally designed and synthesized by using anionic bis(oxalato)chromate(III) mononuclear complexes, $[Cr^{III}L(ox)_2]^-$, as bidentate metalloligands toward cationic cobalt(II) mononuclear complexes, $[Co^{II}L'(H_2O)_4]^{2+}$, where L and L′ are aromatic α,α'-diimine blocking ligands like 2,2′-bipyridine (bpy) and 1,10-phenanthroline (phen) or their sterically hindered β,β'-dimethyl-substituted derivatives 6,6′-dimethyl-2,2′-bipyridine (Me_2bpy) and 2,9-dimethyl-1,10-phenanthroline (Me_2phen) (Charts 1a and 1b).[21] In the present paper, we show that this approach can be further extended to the preparation of homo- and heteroleptic, ferromagnetically coupled chromium(III)-cobalt(II) and chromium(III)-manganese(II) dinuclear complexes, $[Cr^{III}L(ox)_2M^{II}L'(H_2O)_2]^+$, where the two coordinated water molecules occupy either *trans* (M = Co) or *cis* (M = Mn) positions (Charts 1c and 1d, respectively).

Chart 1. Bis(oxalato)chromate(III) Mononuclear Precursors (a) and Resulting Oxalato-Bridged Chromium(III)-Cobalt(II) and Chromium(III)-Manganese(II) Tri- (b) and Dinuclear Complexes (c and d) with Various Aromatic Diimine Blocking Ligands[a]

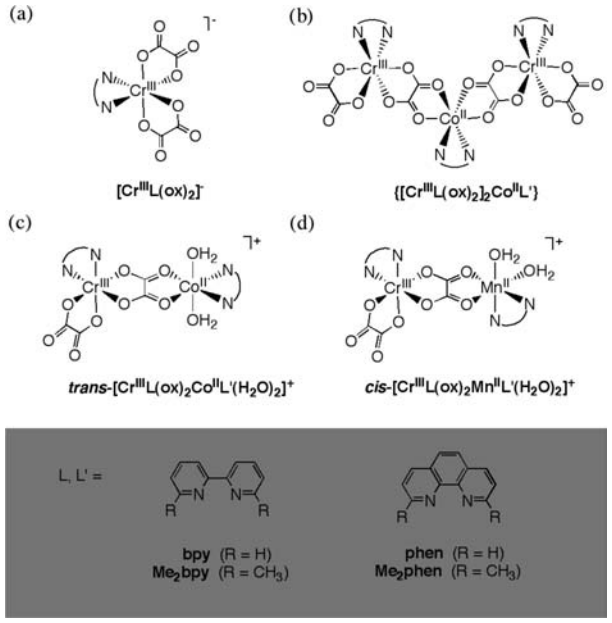

[a]See the boxed structure.

Herein we report the syntheses, crystal structures, and magnetic properties of the bis(oxalato)chromate(III) mononuclear salts of such two novel oxalato-bridged chromium(III)-cobalt(II) and chromium(III)-manganese(II) dinuclear complexes of formula $[Cr(bpy)(ox)_2Co(Me_2phen)(H_2O)_2][Cr(bpy)(ox)_2]\cdot 4H_2O$ (**1**) and $[Cr(phen)(ox)_2Mn(phen)(H_2O)_2][Cr(phen)(ox)_2]\cdot H_2O$ (**2**), respectively. In a preliminar communication,[21b] we showed that complex **1** exhibits an intriguing solvatomagnetic behavior

dx.doi.org/10.1021/ic202755z | Inorg. Chem. 2012, 51, 3289−3301

upon further removal of the two coordinated water molecules to give the corresponding trinuclear chromium(III)-cobalt(II) complex of formula $\{[Cr(bpy)(ox)_2]_2Co(Me_2phen)\}$, which constitutes one of the few examples of single molecule magnets (SMMs) belonging to the class of heterobimetallic oxalates.[22] Now we focus on a theoretical analysis of the nature and magnitude of the magnetic coupling for **1** and **2** in the light of accurate electronic structure calculations. In this respect, it deserves to be noted that these two new oxalato-bridged heterodinuclear complexes with aromatic diimine-type blocking ligands constitute the simplest model systems for the study of the electron exchange interactions through the oxalato bridge in a discrete $Cr^{III}M^{II}$ entity (M = Co and Mn), both from experimental and theoretical viewpoints.

EXPERIMENTAL SECTION

Materials. All chemicals were of reagent grade quality. They were purchased from commercial sources and used as received. The bis(oxalato)chromate(III) mononuclear precursors of formula $Ph_4P[Cr(bpy)(ox)_2]\cdot H_2O$ and $Ph_4P[Cr(phen)(ox)_2]\cdot H_2O$ were synthesized by following previously reported procedures.[18a,23]

$[Cr(bpy)(ox)_2Co(Me_2phen)(H_2O)_2][Cr(bpy)(ox)_2]\cdot 4H_2O$ (1). A methanolic solution (10 cm^3) of $Me_2phen\cdot 1/2H_2O$ (0.10 g, 0.5 mmol) was added dropwise to an aqueous solution (5 cm^3) of $Co(NO_3)_2\cdot 6H_2O$ (0.15 g, 0.5 mmol) under continuous stirring. The resulting deep orange solution was then added dropwise to a methanolic solution (35 cm^3) of $Ph_4P[Cr(bpy)(ox)_2]\cdot H_2O$ (0.74 g, 1.0 mmol) under continuous stirring. The final deep pink solution was filtered off and allowed to evaporate at room temperature. X-ray quality red prisms of **1** appeared after a few days, which were collected on filter paper and air-dried (yield: 35%). *Anal.* calc. for $C_{42}H_{40}CoCr_2N_6O_{22}$: C, 44.07; H, 3.50; N, 7.34%. Found: C, 45.05; H, 3.59; N, 7.38%. IR (KBr): 1717, 1705, 1685, and 1670 cm^{-1} (C═O).

$[Cr(phen)(ox)_2Mn(phen)(H_2O)_2][Cr(phen)(ox)_2]\cdot H_2O$ (2). A methanolic solution (10 cm^3) of phen (0.09 g, 0.5 mmol) was added dropwise to an aqueous solution (5 cm^3) of $Mn(NO_3)_2\cdot 4H_2O$ (0.13 g, 0.5 mmol) under continuous stirring. The resulting pale yellow solution was then added dropwise to a methanolic solution (35 cm^3) of $Ph_4P[Cr(phen)(ox)_2]\cdot H_2O$ (0.77 g, 1.0 mmol) under continuous stirring. The final deep pink solution was filtered off and allowed to evaporate at room temperature. X-ray quality pink rhombs of **2** appeared after a few days, which were collected on filter paper and air-dried (yield: 30%). *Anal.* calc. for $C_{42}H_{40}CoCr_2N_6O_{22}$: C, 47.80; H, 2.73; N, 7.60%. Found: C, 48.43; H, 2.74; N, 7.56%. IR (KBr): 1717, 1700, 1680, and 1662 cm^{-1} (C═O).

Physical Techniques. Elemental (C, H, and N) analyses were performed at the Servei Central de Suport a la Investigació Experimental (SCSIE, Spain). FTIR spectra were recorded on a Nicolet-5700 spectrophotometer as KBr pellets. Variable-temperature (2.0−300 K) magnetic susceptibility measurements under an applied field of 10 kOe ($T \geq 25$ K) and 100 Oe ($T < 25$ K) and variable-field (H = 0−50 kOe) magnetization measurements at 2.0 K were carried out on powdered samples with a Quantum Design SQUID magnetometer. The susceptibility data were corrected for the diamagnetism of the sample holder and the constituent atoms, as well as for the temperature-independent paramagnetism (TIP) of the metal atoms.

Crystal Data Collection and Refinement. The single-crystal X-ray diffraction data of **1** and **2** were collected at 293(2) K on a Nonius Kappa CCD diffractometer by using graphite-monochromated Mo-K_α radiation (λ = 0.71073 Å). Data collection and data reduction were done with the COLLECT and EVALCCD programs.[24] Empirical absorption corrections were carried out using SADABS.[25] The structures were solved by direct methods and refined with full-matrix least-squares technique on F^2 using the SHELXS-97 and SHELXL-97 programs.[26] All calculations for data reduction, structure solution, and refinement were done by standard procedures (WINGX).[27] All non-hydrogen atoms were refined anisotropically. Hydrogen atoms were calculated and refined with an overall isotropic thermal parameter (except for those of the crystallization water molecules, which were neither found nor calculated). The final geometrical calculations and the graphical manipulations were carried out with PARST97 and CRYSTAL MAKER programs, respectively.[28]

Computational Details. Density functional (DF) calculations on **1** and **2** in the gas phase and in solution were carried out with the hybrid B3LYP method[29] combined with the broken-symmetry (BS) approach,[30] as implemented in the Gaussian 09 program.[31] The molecular geometries of the dinuclear model molecules were not optimized, but their bond lengths and interbond angles were taken from the actual structures determined by single-crystal X-ray diffraction. The triple- and double-ζ quality basis sets proposed by Ahlrichs and co-workers were used for the metal and nonmetal atoms, respectively.[32] Solvation effects were introduced by using a polarizable continuum model (PCM) with parameters corresponding to both acetonitrile and dichloromethane solvents.[33] The energy of the "true" lowest spin configuration was not obtained by the projection of the BS wave function, but they were considered equivalent for the evaluation of the magnetic coupling parameter. The calculated spin density data were obtained from natural bond orbital (NBO) analysis.[34] DF periodic calculations were done on the experimental crystal cell of **1** and **2** with the SIESTA (Spanish Initiative for Electronic Simulations with Thousands of Atoms) program[35] by using the revised GGA exchange-correlation functional of Perdew, Burke, and Erzernhof (RPBE) proposed by Hammer et al.[36] Values of 50 meV and 200 Ry were selected for the energy shift and mesh cutoff, respectively, which provide a good compromise between accuracy and computer time needed to calculate the magnetic coupling parameters.[37] Only valence electrons were included in the calculations, the cores being replaced by norm-conserving scalar relativistic pseudopotentials which were factorized in the Kleinman-Bylander form.[38] These pseudopotentials were generated from the ground state atomic configurations of all atoms following the approach proposed by Trouiller and Martins.[39] The values of the core radii for the s, p, d, and f components of the metal atoms were 2.61, 2.61, 2.45, and 2.45 (Cr), 2.10, 2.10, 1.78, and 2.10 (Co), and 2.51, 2.57, 2.38, and 2.38 (Mn), respectively. The values of the cutoff radii for all the s, p, d, and f components of the nonmetal atoms were 1.47 (O), 1.48 (N), 1.56 (C), and 1.33 (H). Several fineness values of the k-grid for the Brillouin zone sampling were used in **1**. Since similar results for the magnetic coupling were obtained in all cases, only a single k-point was used in **2**.

RESULTS AND DISCUSSION

Description of the Structures. The crystal structures of **1** and **2** consist of oxalato-bridged chromium(III)-cobalt(II) and chromium(III)-manganese(II) heterodinuclear cations, $[Cr^{III}L(ox)(\mu\text{-}ox)M^{II}L'(H_2O)_2]^+$ [M = Co, L = bpy, and L′ = Me_2phen (**1**); M = Mn and L = L′ = phen (**2**)], bis(oxalato)chromate(III) mononuclear anions, $[Cr^{III}L(ox)_2]^-$ [L = bpy (**1**) and phen (**2**)], and crystallization water molecules (Figures 1 and 2). A summary of the crystallographic data for **1** and **2** is given in Table 1. Selected bond distances and angles for **1** and **2** are listed in Tables 2 and 3, respectively.

The $Cr^{III}M^{II}$ dinuclear cations of **1** (M = Co) and **2** (M = Mn) arise from the bidentate coordination of one of the two $[Cr^{III}L(ox)_2]^-$ units [L = bpy (**1**) and phen (**2**)] through one ofits two oxalato groups toward a $[M^{II}L'(H_2O)_2]^{2+}$ moiety [M = Co and L′ = Me_2phen (**1**); M = Mn and L′ = phen (**2**)] with either *trans* (**1**) or *cis* (**2**) disposition of the two coordinated water molecules (Figures 1a and 2a, respectively). This situation contrasts with that found in the related oxalato-bridged heterotrinuclear cobalt(II)-chromium(III) complex of formula $\{[Cr^{III}(phen)(ox)_2]_2Co^{II}(Me_2bpy)_2\}\cdot 1.5H_2O$, whereby the two $[Cr^{III}(phen)(ox)_2]^-$ units coordinate to the $[Co^{II}(Me_2bpy)_2]^{2+}$ moiety in a bidentate manner to give discrete $Co^{II}Cr^{III}_2$ bent entities.[21a] The values of the intramolecular Cr(1)−M(1) distance (M = Co and Mn) across the oxalato bridge are 5.423(2) (**1**) and 5.3894(10) Å (**2**).

The two crystallographically independent Cr(1) and Cr(2) atoms in **1** and **2** adopt a more or less trigonally compressed

dx.doi.org/10.1021/ic202755z | Inorg. Chem. 2012, 51, 3289−3301

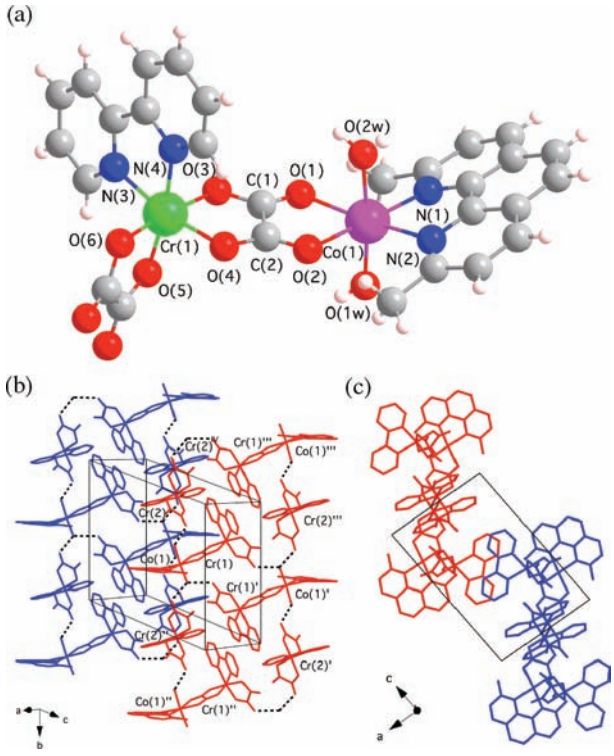

Figure 1. (a) Perspective view of the cationic dinuclear unit of **1** with the atom-numbering scheme. (b) Perspective view of two adjacent ladder-like chains of hydrogen-bonded mono- and dinuclear units of **1** [symmetry codes: (I) = 1 − *x*, 1 − *y*, − *z*; (II) = *x*, *y* − 1, *z*; (III) = 1 − *x*, 2 − *y*, − *z*; (IV) = *x*, 1 + *y*, *z*]. Hydrogen bonds are represented by dashed lines. (c) Crystal packing view of **1** along the *b* axis showing the π-π stacking interactions between adjacent chains (shown in different colors).

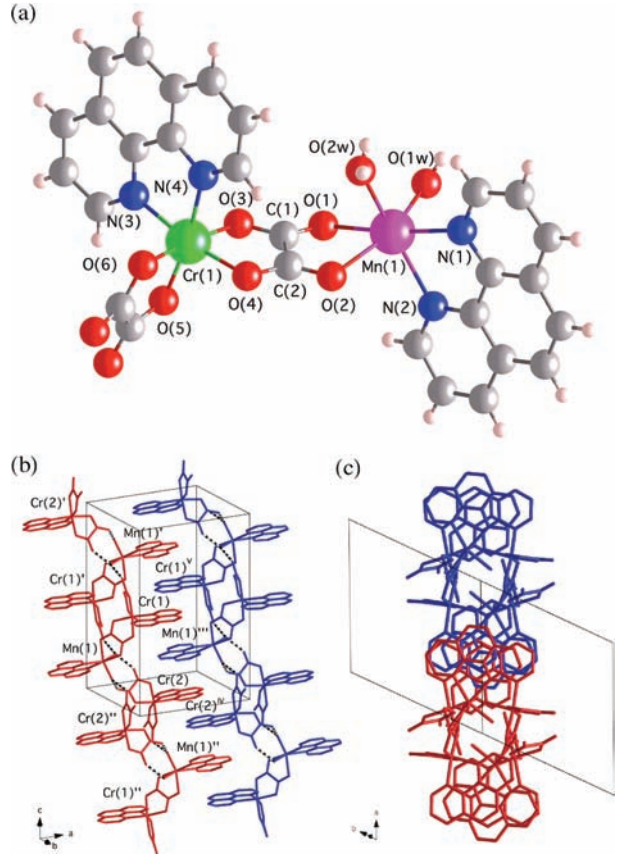

Figure 2. (a) Perspective view of the cationic dinuclear unit of **2** with the atom-numbering scheme. (b) Perspective view of two adjacent ribbon-like chains of hydrogen-bonded mono- and dinuclear units of **2** [symmetry code: (I) = − *x*, − *y* − 1, 1 − *z*; (II) = − *x*, − *y*, − *z*; (III) = 1 + *x*, *y*, *z*; (IV) = 1 − *x*, − *y*, − *z*; (V) = 1 − *x*, − 1 − *y*, 1 − *z*]. Hydrogen bonds are represented by dashed lines. (c) Crystal packing view of **2** along the [0,−1,−1] direction showing the π-π stacking interactions between adjacent chains (shown in different colors).

octahedral geometry. The CrN_2O_4 environment is formed by two imine-nitrogen atoms from bpy (**1**) and phen (**2**), and four carboxylate-oxygen atoms from the two oxalates. The values of the trigonal twist angle at Cr(1) [ϕ = 49.23 (**1**) and 50.75° (**2**)] are smaller than those at Cr(2) [ϕ = 57.35 (**1**) and 56.61° (**2**)], while the values of the compression ratio at Cr(1) [*s*/*h* = 1.307 (**1**) and 1.303 (**2**)] are greater than those at Cr(2) [*s*/*h* = 1.265 (**1**) and 1.230 (**2**)] (ϕ = 60° and *s*/*h* = $\sqrt{3}/2$ = 1.22 for an ideal octahedron).[40] The larger distortion of the octahedral (O_h) environment of the Cr^{III} ions from the $Cr^{III}M^{II}$ dinuclear cations toward trigonal prismatic (D_{3h}), so-called Bailar twist, reflects the importance of the steric requirements upon coordination to the M^{II} ion in **1** (M = Co) and **2** (M = Mn). The metal−ligand bond distances from bpy and phen are similar [Cr−N = 2.054(3)−2.067(3) (**1**) and 2.052(3)−2.080(3) Å (**2**), respectively], being somewhat larger than those from oxalate [Cr−O = 1.938(3)−2.005(3) (**1**) and 1.924(2)−1.997(2) Å (**2**)]. This situation agrees with the stronger ligand field of the carboxylate-oxygen atoms compared to the imine-nitrogen ones, as previously observed in $Ph_4P[CrL(ox)_2]\cdot H_2O$ (L = bpy and phen) [Cr−N = 2.057(3)−2.083(4) Å and Cr−O = 1.946(2)−1.960(2) Å].[20a,23b] Interestingly, the average values of the chromium to oxygen bond distances from the bridging oxalate [Cr−O = 1.996(3) (**1**) and 1.986(2) Å (**2**)] are slightly greater than those from the terminal ones [Cr−O = 1.952(3) (**1**) and 1.947(2) Å (**2**)], reflecting thus the differences in the electronic delocalization onto the oxalato bridge upon coordination to the M^{II} ion in **1** (M = Co) and **2** (M = Mn). The values of the bite angle subtended by the chelating bpy and phen [N−Cr−N = 78.69(13)−78.71(14) (**1**) and 79.23(11)−80.62(10)° (**2**)] are somewhat smaller than those from oxalate [O−Cr−O = 82.46(10)−83.36(11) (**1**) and 82.75(10)−83.61(9)° (**2**)], both of them being smaller than that of an ideal octahedron (90°).

The Co(1) atom in **1** exhibits an axially compressed octahedral environment, CoN_2O_4, whereby two imine-nitrogen atoms from Me_2phen and two carbonyl-oxygen atoms from the bridging oxalate define the equatorial plane while two *trans*-diaqua oxygen atoms occupy the axial positions. The axial metal−ligand bond distances from water [Co−Ow = 2.029(3)−2.088(3) Å] are rather shorter than the equatorial ones from Me_2phen [Co−N = 2.149(3)−2.151(3) Å] and oxalate [Co−O = 2.152(3)−2.179(2) Å], all of them being typical of a high-spin Co^{II} ion. The value of the metal−ligand bond angle from the two *trans* axial water molecules [Ow−Co−Ow = 174.83(14)°] slightly deviates from that of an ideal octahedron (180°). The value of the bite angle subtended by the chelating Me_2phen [N−Co−N = 78.39(10)°] is similar to that from oxalate [O−Co−O = 77.08(9)°], both of them being significantly smaller than that of an ideal octahedron (90°). This equatorial bending results in an additional rhombic (D_{2h}) distortion of the axially compressed octahedral environment of the high-spin Co^{II} ion in **1**. On the contrary, the Mn(1) atom in **2** shows a trigonally compressed octahedral environment, MnN_2O_4, which is built up by two imine-nitrogen atoms from

dx.doi.org/10.1021/ic202755z | *Inorg. Chem.* 2012, 51, 3289−3301

Table 1. Summary of Crystallographic Data for 1 and 2

	1	2
formula	$C_{42}H_{40}CoCr_2N_6O_{22}$	$C_{44}H_{30}Cr_2MnN_6O_{19}$
M/g mol^{-1}	1143.73	1105.68
crystal system	triclinic	triclinic
space group	$P\bar{1}$	$P\bar{1}$
a/Å	10.180(4)	10.9438(9)
b/Å	14.653(5)	11.0838(13)
c/Å	16.585(13)	20.525(3)
α/deg	72.900(12)	80.592(11)
β/deg	83.494(12)	81.995(11)
γ/deg	87.647(6)	64.037(7)
V/Å^3	2349(2)	2201.9(5)
Z	2	2
ρ_{calc}/g cm^{-3}	1.617	1.668
$F(000)$	1170	1122
μ/mm^{-1}	0.895	0.857
T/K	293(2)	293(2)
reflect. collcd.	28488	23204
reflect. indep. (R_{int})	11672 (0.0428)	10181 (0.0498)
reflect. obs. [$I > 2\sigma(I)$]	8582	7348
data/restraints/parameters	11672/0/692	10181/0/665
R_1[a] [$I > 2\sigma(I)$] (all)	0.0644 (0.0952)	0.0641 (0.0997)
wR_2[b] [$I > 2\sigma(I)$] (all)	0.1362 (0.1519)	0.1159 (0.1319)
S[c]	1.051	1.079

[a] $R_1 = \sum||F_o| - |F_c||/\sum|F_o|$. [b] $wR_2 = [\sum w(F_o^2 - F_c^2)^2/\sum w(F_o^2)^2]^{1/2}$. [c] $S = [\sum w(|F_o| - |F_c|)^2/(N_o - N_p)]^{1/2}$.

phen, two carbonyl-oxygen atoms from the bridging oxalate, and two *cis*-diaqua oxygen atoms [ϕ = 53.84° and s/h = 1.499]. The metal−ligand bond distances from water [Mn−Ow = 2.078(3)−2.179(3) Å] are slightly shorter than those from phen [Mn−N = 2.243(3)−2.277(3) Å] and oxalate [Mn−O = 2.196(2)−2.306(2) Å]. The value of the metal−ligand bond angle from the two *cis* water molecules [Ow−Co−Ow = 94.21(16)°] is significantly larger than those of the bite angle from phen [N−Mn−N = 73.03(12)°] and oxalate [O−Cr−O = 73.96(8)°], all of them deviating appreciably from that for an ideal octahedron (90°). Overall, this situation leads to an additional (C_2) distortion of the trigonally compressed octahedral environment of the high-spin Mn^{II} ion in **2**.

In the crystal lattice, the Cr^{III} mononuclear anions and the $Cr^{III}M^{II}$ dinuclear cations of **1** (M = Co) and **2** (M = Mn) establish a variety of hydrogen bonds involving the free carbonyl groups from oxalate and the coordinated water molecules [O−Ow = 2.712(4)−2.774(4) (**1**) and 2.649(4)−2.844(5) Å (**2**)]. These intermolecular interactions lead to hydrogen-bonded chains with either ladder- (**1**) or ribbon-like (**2**) architectures running along the [010] and [0−1−1] directions, respectively (Figures 1b and 2b). In addition, weak π-π stacking intrachain interactions between the bpy ligands from each pair of centrosymmetrically related $Cr^{III}Co^{II}$ dinuclear cations occur in **1** [inter-ring centroid-centroid distance of 3.839(2) Å]. The value of the intrachain $Cr(1)−Cr(1)^{III}$ distance across this π-π stacking bpy−bpy motif in **1** is 7.798(3) Å. The values of the intrachain $M(1)−Cr(2)$, $M(1)−Cr(1)^{I}$, and $M(1)−Cr(2)^{II}$ distances (M = Co and Mn) through the hydrogen-bonded bridging motifs in **1** are 7.880(3), 7.778(3), and 7.958(3) Å, while the corresponding ones in **2** are 7.2102(12), 6.7038(12), and 7.2355(13) Å, respectively.

On the other hand, the packing of the hydrogen-bonded chains in **1** and **2** leads to a layer array of interdigitated ladder (**1**) and ribbon (**2**) chains along the crystallographic c and a axes, respectively (Figures 1c and 2c). This zipper-type packing involves single π-π stacking interchain interactions between the bpy ligands from each pair of centrosymmetrically related Cr^{III} mononuclear anions in **1** [inter-ring centroid-centroid distance of 3.9018(11) Å] (Figure 1b), whereas it consists of multiple π-π stacking interchain interactions between the phen ligands from each pair of centrosymmetrically related Cr^{III} mononuclear anions and $Cr^{III}Mn^{II}$ dinuclear cations in **2** [inter-ring centroid-centroid distances in the range of 3.4719(5)−3.8703(6) Å] (Figure 2b). The value of the interchain $Cr(2)−Cr(2)^{IV}$ distance across the bpy−bpy stacking motif in **1** is 7.417(3) Å, while those of the interchain $Cr(1)−Mn(1)^{III}$, $Cr(2)−Mn(1)^{III}$, $Cr(2)−Cr(2)^{IV}$, and $Cr(1)−Cr(1)^{V}$ distances through the phen−phen stacking motifs in **2** are 8.5233(12), 8.7100(13), 9.2135(13), and 8.9115(12) Å, respectively.

Table 2. Selected Bond Distances (Å) and Angles (deg) for 1[a]

Cr(1)−N(3)	2.062(3)	Cr(2)−N(5)	2.061(4)
Cr(1)−N(4)	2.054(3)	Cr(2)−N(6)	2.067(3)
Cr(1)−O(3)	2.005(3)	Cr(2)−O(9)	1.964(3)
Cr(1)−O(4)	1.987(2)	Cr(2)−O(10)	1.972(2)
Cr(1)−O(5)	1.940(2)	Cr(2)−O(13)	1.956(3)
Cr(1)−O(6)	1.941(3)	Cr(2)−O(14)	1.938(3)
Co(1)−N(1)	2.151(3)	Co(1)−N(2)	2.149(3)
Co(1)−O(1)	2.179(2)	Co(1)−O(2)	2.152(3)
Co(1)−O(1w)	2.029(3)	Co(1)−O(2w)	2.088(3)
N(3)−Cr(1)−N(4)	78.69(13)	N(5)−Cr(2)−N(6)	78.71(14)
N(3)−Cr(1)−O(3)	91.34(11)	N(5)−Cr(2)−O(9)	95.40(12)
N(3)−Cr(1)−O(4)	92.94(12)	N(5)−Cr(2)−O(10)	94.84(12)
N(3)−Cr(1)−O(5)	171.88(12)	N(5)−Cr(2)−O(13)	91.16(12)
N(3)−Cr(1)−O(6)	92.37(12)	N(5)−Cr(2)−O(14)	169.95(12)
N(4)−Cr(1)−O(3)	88.40(11)	N(6)−Cr(2)−O(9)	169.13(12)
N(4)−Cr(1)−O(4)	167.48(11)	N(6)−Cr(2)−O(10)	88.68(11)
N(4)−Cr(1)−O(5)	95.00(12)	N(6)−Cr(2)−O(13)	96.26(12)
N(4)−Cr(1)−O(6)	97.65(12)	N(6)−Cr(2)−O(14)	93.95(14)
O(3)−Cr(1)−O(4)	82.46(10)	O(9)−Cr(2)−O(10)	82.68(10)
O(3)−Cr(1)−O(5)	93.59(10)	O(9)−Cr(2)−O(13)	92.96(11)
O(3)−Cr(1)−O(6)	173.43(11)	O(9)−Cr(2)−O(14)	92.91(12)
O(4)−Cr(1)−O(5)	94.09(11)	O(10)−Cr(2)−O(13)	172.88(11)
O(4)−Cr(1)−O(6)	91.93(11)	O(10)−Cr(2)−O(14)	91.81(12)
O(5)−Cr(1)−O(6)	83.36(11)	O(13)−Cr(2)−O(14)	82.76(12)
N(1)−Co(1)−N(2)	78.39(10)	N(1)−Co(1)−O(1)	103.72(9)
N(1)−Co(1)−O(2)	177.20(10)	N(1)−Co(1)−O(1w)	93.02(13)
N(1)−Co(1)−O(2w)	90.31(11)	N(2)−Co(1)−O(1)	171.83(9)
N(2)−Co(1)−O(2)	100.44(10)	N(2)−Co(1)−O(1w)	97.56(12)
N(2)−Co(1)−O(2w)	86.98(11)	O(1)−Co(1)−O(2)	77.08(9)
O(1)−Co(1)−O(1w)	90.24(11)	O(1)−Co(1)−O(2w)	85.12(11)
O(2)−Co(1)−O(1w)	89.65(13)	O(2)−Co(1)−O(2w)	87.09(11)
O(1w)−Co(1)−O(2w)	174.83(14)		

[a] Estimated standard deviations are given in parentheses.

Magnetic Properties. The magnetic properties of **1** and **2** in the form of the χT vs T (χ being the molar magnetic susceptibility and T the absolute temperature) and the M vs H plots (M being the molar magnetization and H the applied field) are shown in Figures 3 and 4, respectively.

The χT vs T plots of **1** and **2** show a qualitatively similar magnetic behavior, which is consistent with their mononuclear plus dinuclear structures (Figure 3). At room temperature, χT is equal to 5.82 (**1**) and 8.20 cm^3 mol^{-1} K (**2**), values which are close to those expected for the sum of two d^3 Cr^{III} (S_{Cr} = 3/2)

dx.doi.org/10.1021/ic202755z | Inorg. Chem. 2012, 51, 3289−3301

Table 3. Selected Bond Distances (Å) and Angles (deg) for 2[a]

Cr(1)−N(3)	2.053(3)	Cr(2)−N(5)	2.080(3)
Cr(1)−N(4)	2.062(3)	Cr(2)−N(6)	2.052(3)
Cr(1)−O(3)	1.997(2)	Cr(2)−O(9)	1.952(2)
Cr(1)−O(4)	1.974(2)	Cr(2)−O(10)	1.968(2)
Cr(1)−O(5)	1.924(2)	Cr(2)−O(13)	1.958(2)
Cr(1)−O(6)	1.951(2)	Cr(2)−O(14)	1.931(2)
Mn(1)−N(1)	2.277(3)	Mn(1)−N(2)	2.243(3)
Mn(1)−O(1)	2.306(2)	Mn(1)−O(2)	2.196(2)
Mn(1)−O(1w)	2.078(3)	Mn(1)−O(2w)	2.179(3)
N(3)−Cr(1)−N(4)	80.62(10)	N(5)−Cr(2)−N(6)	79.23(11)
N(3)−Cr(1)−O(3)	91.87(9)	N(5)−Cr(2)−O(9)	92.88(11)
N(3)−Cr(1)−O(4)	170.73(10)	N(5)−Cr(2)−O(10)	91.66(11)
N(3)−Cr(1)−O(5)	92.62(10)	N(5)−Cr(2)−O(13)	92.46(11)
N(3)−Cr(1)−O(6)	93.72(9)	N(5)−Cr(2)−O(14)	173.01(11)
N(4)−Cr(1)−O(3)	91.28(10)	N(6)−Cr(2)−O(9)	169.74(11)
N(4)−Cr(1)−O(4)	91.74(10)	N(6)−Cr(2)−O(10)	90.88(10)
N(4)−Cr(1)−O(5)	171.46(10)	N(6)−Cr(2)−O(13)	93.89(11)
N(4)−Cr(1)−O(6)	91.58(9)	N(6)−Cr(2)−O(14)	95.30(11)
O(3)−Cr(1)−O(4)	83.00(9)	O(9)−Cr(2)−O(10)	82.75(10)
O(3)−Cr(1)−O(5)	94.16(10)	O(9)−Cr(2)−O(13)	92.98(11)
O(3)−Cr(1)−O(6)	174.07(9)	O(9)−Cr(2)−O(14)	93.04(11)
O(4)−Cr(1)−O(5)	95.44(10)	O(10)−Cr(2)−O(13)	174.20(10)
O(4)−Cr(1)−O(6)	91.72(9)	O(10)−Cr(2)−O(14)	92.77(10)
O(5)−Cr(1)−O(6)	83.61(9)	O(13)−Cr(2)−O(14)	83.53(10)
N(1)−Mn(1)−N(2)	73.03(12)	N(1)−Mn(1)−O(1)	174.67(11)
N(1)−Mn(1)−O(2)	109.60(10)	N(1)−Mn(1)−O(1w)	92.50(13)
N(1)−Mn(1)−O(2w)	87.94(12)	N(2)−Mn(1)−O(1)	111.53(11)
N(2)−Mn(1)−O(2)	86.20(9)	N(2)−Mn(1)−O(1w)	104.76(14)
N(2)−Mn(1)−O(2w)	153.43(13)	O(1)−Mn(1)−O(2)	73.96(8)
O(1)−Mn(1)−O(1w)	83.71(12)	O(1)−Mn(1)−O(2w)	88.60(11)
O(2)−Mn(1)−O(1w)	157.52(12)	O(2)−Mn(1)−O(2w)	82.88(12)
O(1w)−Mn(1)−O(2w)	94.21(16)		

[a]Estimated standard deviations are given in parentheses.

ions and one high-spin d^7 Co^{II} (S_{Co} = 3/2) or d^5 Mn^{II} (S_{Mn} = 5/2) ion, respectively [$\chi T = 2 \times (N\beta^2 g_{Cr}{}^2/3k_B)S_{Cr}(S_{Cr} + 1) + (N\beta^2 g_M{}^2/3k_B)S_M(S_M + 1)$ = 5.82 (**1**) and 8.13 cm^3 mol^{-1} K (**2**) with g_{Cr} = 2.0 and $g_M = g_{Co}$ = 2.1 and $g_M = g_{Mn}$ = 2.0]. Upon cooling, χT continuously increases to reach a maximum of 6.14 (**1**) and 9.87 cm^3 mol^{-1} K (**2**) at 14.0 (**1**) and 4.0 K (**2**), and then it abruptly decreases down to 5.05 (**1**) and 8.88 cm^3 mol^{-1} K (**2**) at 2.0 K. The increase of χT in the high temperature region for **1** and **2** indicates a weak intramolecular ferromagnetic interaction between the Cr^{III} (S_{Cr} = 3/2) and the Co^{II} (S_{Co} = 3/2) or Mn^{II} (S_{Mn} = 5/2) ions respectively, across the oxalato bridge within the $Cr^{III}M^{II}$ dinuclear entities (M = Co and Mn). Yet the maximum values of χT for **1** and **2** are well below those expected for a S_{Cr} = 3/2 from the Cr^{III} mononuclear unit plus a $S_{CrM} = S_{Cr} + S_M$ = 3 (M = Co) or 4 (M = Mn) ground spin state, respectively [$\chi T = (N\beta^2 g_{Cr}{}^2/3k_B)S_{Cr}(S_{Cr} + 1) + (N\beta^2 g_{CrM}{}^2/3k_B)S_{CrM}(S_{CrM} + 1)$ = 8.18 (**1**) or 11.88 cm^3 mol^{-1} K (**2**) with $g_{CrM} = g_{CrCo} = (g_{Co} + g_{Cr})/2$ = 2.05 and $g_{CrM} = g_{CrMn} = (5g_{Mn} + 3g_{Cr})/8$ = 2.0]. The decrease of χT in the low temperature region for **1** and **2** is most likely due to zero-field splitting (ZFS) effects and/or intermolecular antiferromagnetic interactions.

In fact, the M vs H plots for **1** and **2** at 2.0 K agree with the presence of more or less anisotropic, weak ferromagnetically coupled $Cr^{III}M^{II}$ dinuclear entities (M = Co and Mn) and Cr^{III} mononuclear units (Figure 4). The M value of 8.18 $N\beta$ for **1** at 50 kOe is slightly below the saturation magnetization for the sum

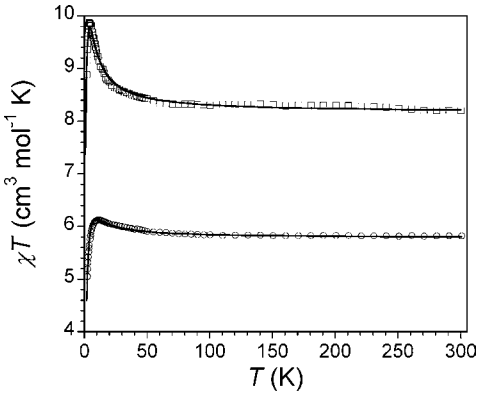

Figure 3. Temperature dependence of χT for **1** (○) and **2** (□). The solid lines are the best-fit curves (see text).

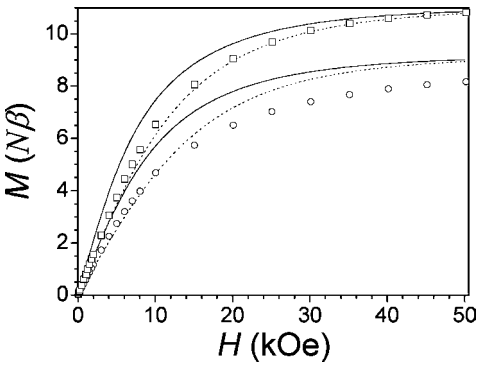

Figure 4. Field dependence of M for **1** (○) and **2** (□) at T = 2.0 K. The solid lines are the Brillouin curves for one S_{Cr} = 3/2 state plus one S_{CrM} = 3 (M = Co) or 4 (M = Mn) state, while the dotted lines are the Brillouin curves for two S_{Cr} = 3/2 states plus one S_M = 3/2 (M = Co) or 5/2 (M = Mn) state (see text).

of two S_{Cr} = 3/2 and one S_{Co} = 3/2 states ($M_s = 2 \times g_{Cr}S_{Cr} + g_{Co}S_{Co}$ = 9.15 $N\beta$ with g_{Cr} = 2.0 and g_{Co} = 2.1), supporting thus the presence of a significant single-ion axial magnetic anisotropy of the high-spin octahedral Co^{II} ion ($^4T_{1g}$ ground term in the O_h point group). Moreover, the isothermal magnetization curve at low H values (H < 10 kOe) for **1** is intermediate between the Brillouin curves of three quartet states ($S_{Cr} = S_{Co}$ = 3/2) and one quartet (S_{Cr} = 3/2) plus one septet (S_{CrCo} = 3) spin states (dotted and solid lines respectively, in Figure 4). This feature indicates the proximity of low-lying excited states with spin values smaller than the S_{CrCo} = 3 ground spin state which are thermally populated in this low temperature region. In the absence of ZFS, there are three S_{CrCo} = 2, 1, and 0 excited states close in energy to the S_{CrCo} = 3 ground state which are located at 3J, 5J, and 6J, respectively. By contrast, the M value of 10.83 $N\beta$ for **2** at 50 kOe is close to the saturation magnetization for the sum of two S_{Cr} = 3/2 and one S_{Mn} = 5/2 states ($M_s = 2 \times g_{Cr}S_{Cr} + g_{Mn}S_{Mn}$ = 11.0 $N\beta$ with g_{Cr} = 2.0 and g_{Mn} = 2.0), as expected from the almost negligible single-ion axial magnetic anisotropy of the high-spin octahedral Mn^{II} ion ($^6A_{1g}$ ground term in the O_h point group). Yet the isothermal magnetization curve for **2** is intermediate between the Brillouin curves of two quartet (S_{Cr} = 3/2) plus one sextet (S_{Mn} = 5/2) spin states and one quartet (S_{Cr} = 3/2) plus one nonet (S_{CrMn} = 4) spin states (dotted and solid lines respectively, in Figure 4). Once again, this fact indicates the proximity of low-lying excited states with smaller spin values than the S_{CrMn} = 4 ground state which are thermally populated at 2.0 K (*v.g.*, the three

dx.doi.org/10.1021/ic202755z | Inorg. Chem. 2012, 51, 3289−3301

S_{CrMn} = 3, 2, and 1 excited states which are located at 4*J*, 7*J*, and 9*J* above the S_{CrMn} = 4 ground state).

The magnetic susceptibility data of **1** and **2** were first analyzed through a spin Hamiltonian for a mononuclear plus dinuclear model that takes into account the presence of weak intermolecular interactions between the dinuclear entities within the mean field approximation [eq 1 with $S_{Cr1} = S_{Cr2} = 3/2$ and $S_{M1} = 3/2$ (M = Co) or 5/2 (M = Mn)], where *J* and *j* are the intra- and intermolecular magnetic coupling parameters respectively, *z* is the number of magnetic neighbors, and g_{Cr} and g_M are the Landé factors of the Cr^{III} and M^{II} ions (M = Co and Mn).

$$\mathbf{H} = -J\mathbf{S_{Cr1}}\cdot\mathbf{S_{M1}} + zj\langle\mathbf{S_{CrM(z)}}\rangle\mathbf{S_{CrM(z)}} + g_{Cr}(\mathbf{S_{Cr1}} + \mathbf{S_{Cr2}})\beta H + g_M\mathbf{S_{M1}}\beta H \quad (1)$$

The least-squares fits of the experimental data of **1** and **2** through the appropriate expression [eq 2, where *N* is the Avogadro number, β is the Bohr magneton, k_B is the Boltzmann constant, $x = J/k_BT$, and θ is the Weiss factor defined as $\theta = zjS_{CrM}(S_{CrM} + 1)/3k_B$], gave J = +2.0 (**1**) and +1.2 cm^{-1} (**2**), zj = −1.1 (**1**) and −0.3 cm^{-1} (**2**), g_{Cr} = 2.00 (**1** and **2**), g_{Co} = 2.06 (**1**), and g_{Mn} = 2.01 (**2**), with $R = 1.5 \times 10^{-5}$ (**1**) and 1.1×10^{-5} (**2**) (Table 4). The theoretical curves closely match the experimental data for **1** and **2** and particularly, they reproduce very well the maximum of χT in the low temperature region (solid lines in Figure 3).

Table 4. Least-Squares Fit Magnetic Parameters for 1 (M = Co) and 2 (M = Mn)

complex	J^a/cm^{-1}	zj^b/cm^{-1}	$D_M{}^c/cm^{-1}$	$g_{Cr}{}^d$	$g_M{}^e$	R^f ($\times 10^5$)
1	+2.0	−1.1	0	2.00	2.06	1.5
	+2.2	−0.2	−0.6	2.00	2.08	0.9
2	+1.2	−0.3	0	2.00	2.01	1.1

[a]Intramolecular magnetic coupling parameter. [b]Product of the number of magnetic neighbors by the intermolecular magnetic coupling parameter. [c]Axial magnetic anisotropy parameter of the M^{II} ions. [d]Landé factor of the Cr^{III} ion. [e]Landé factors of the M^{II} ions (M = Co and Mn). [f]Agreement factor defined as $R = \sum[(\chi_M T)_{exp} - (\chi_M T)_{calcd}]^2/\sum[(\chi_M T)_{exp}]^2$.

$$\chi = \chi_{Cr} + \chi_{CrM} \quad (2)$$

$$\chi_{Cr} = 5N\beta^2 g_{Cr}{}^2/4k_BT \quad (2.1)$$

$$\chi_{CrCo} = [N\beta^2/2k_B(T-\theta)][14(g_{Co}+g_{Cr})^2 + 5(g_{Co}+g_{Cr})^2\exp(-3x) + (g_{Co}+g_{Cr})^2 \times \exp(-5x)]/[7 + 5\exp(-3x) + 3\exp(-5x) + \exp(-6x)] \quad (2.2)$$

$$\chi_{CrMn} = [N\beta^2/8k_B(T-\theta)][(15/2)(5g_{Mn}+3g_{Cr})^2 + (7/18)(17g_{Mn}+7g_{Cr})^2\exp(-4x) + (5/9)(11g_{Mn}+g_{Cr})^2\exp(-7x) + (7g_{Mn}-3g_{Cr})^2\exp(-9x)] /[9 + 7\exp(-4x) + 5\exp(-7x) + 3\exp(-9x)] \quad (2.3)$$

An alternative analysis of the magnetic susceptibility data of **1** was then carried out through a spin Hamiltonian for a mononuclear plus dinuclear model that also takes into account the axial ZFS of the orbital singlet $^4B_{2g}$ ground state of the high-spin Co^{II} ion in a rhombically distorted octahedral geometry (D_{2h} point group) [eq 3 with $S_{Co1} = S_{Cr1} = S_{Cr2} = 3/2$], where *J* and *j* are the intra- and intermolecular magnetic coupling parameters respectively, *z* is the number of magnetic neighbors, D_{Co} is the axial magnetic anisotropy parameter of the Co^{II} ion, and g_{Cr} and g_{Co} are the Landé factors of the Cr^{III} and Co^{II} ions.[41]

$$\mathbf{H} = -J\mathbf{S_{Cr1}}\cdot\mathbf{S_{Co1}} + zj\langle\mathbf{S_{CrCo(z)}}\rangle\mathbf{S_{CrCo(z)}} + D_{Co}\mathbf{S_{Co1(z)}}^2 + g_{Cr}(\mathbf{S_{Cr1}} + \mathbf{S_{Cr2}})\beta H + g_{Co}\mathbf{S_{Co1}}\beta H \quad (3)$$

The least-squares fit of the experimental data of **1** by full-matrix diagonalization techniques[42] gave J = +2.2 cm^{-1}, zj = −0.2 cm^{-1}, D_{Co} = −0.6 cm^{-1}, g_{Cr} = 2.00, and g_{Co} = 2.08, with $R = 0.9 \times 10^{-5}$ (Table 4). Indeed, the quality of the fit was slightly improved when compared to that obtained with $D_{Co} = 0$ as reflected by the lower value of the agreement factor *R*. Yet the calculated value of the axial magnetic anisotropy of the high-spin Co^{II} ion in **1** (D_{Co} = −0.6 cm^{-1}) represents the lower limit given that the intermolecular antiferromagnetic interactions are also included in this model. Thus, the calculated value of the intermolecular antiferromagnetic coupling for **1** according this model (zj = −0.2 cm^{-1}) is similar to that for **2** (zj = −0.3 cm^{-1}) (Table 4). In fact, the intermolecular hydrogen bonding interactions between the $Cr^{III}M^{II}$ dinuclear entities (M = Co and Mn) and/or the Cr^{III} mononuclear units in **1** and **2** are important, and they cannot be neglected, as shown by their crystal structures (see Figures 1b and 2b).

Selected magneto-structural data for **1** and **2** and related oxalato-bridged chromium(III)-metal(II) heteropolynuclear complexes are listed in Table 5.[11,15,16,18−21] In general, a weak intramolecular ferromagnetic coupling is observed (J = 1.0−9.2 cm^{-1}; Table 5, entries 1−7, 10, 15−17, 21, and 23−27), independently of the nature of the M^{II} ion (M = Mn, Fe, Co, Ni, and Cu). However, there are some exceptions that exhibit a weak to moderate intramolecular antiferromagnetic coupling ($-J$ = 0.6−18.8 cm^{-1}; Table 5, entries 8, 9, 11, 13, 14, and 18−20). In this regard, the weak intramolecular ferromagnetic coupling between the Cr^{III} ion and the high-spin M^{II} ion for **1** and **2** [J = +2.2 (M = Co) and +1.2 cm^{-1} (M = Mn); Table 5, entries 1 and 2] contrasts with the situation found in the related series of oxalato-bridged chromium(III)-cobalt(II) and chromium(III)-manganese(II) heteropolynuclear complexes with aromatic diimine ligands, ranging from di- to tri- and tetranuclear species. So, the oxalato-bridged chromium(III)-cobalt(II) trinuclear complexes $\{[Cr(bpy)(ox)_2]_2Co(Me_2bpy)\}\cdot 2H_2O$, $\{[Cr(phen)(ox)_2]_2Co(Me_2bpy)\}\cdot 1.5H_2O$, and $\{[Cr(bpy)(ox)_2]_2Co(Me_2phen)\}$ also exhibit a weak intramolecular ferromagnetic coupling (J = +2.4, +2.3, and +1.8 cm^{-1}; Table 5, entries 15−17).[21] Instead, the oxalato-bridged chromium(III)-manganese(II) di- and tetranuclear complexes $[Cr(phen)(ox)_2Mn(phen)_2(N_3)]\cdot H_2O$ and $\{[Cr(phen)(ox)_2Mn(bpy)(H_2O)]_2(ox)\}\cdot 1.5H_2O$, respectively, show an intramolecular antiferromagnetic coupling (J = −1.9 and −1.1 cm^{-1}; Table 5, entries 11 and 18).[18b,20a] In these two series of oxalato-bridged chromium(III)-cobalt(II) and chromium(III)-manganese(II) polynuclear complexes with aromatic diimine ligands, it appears that the different ferro- or antiferromagnetic nature of the exchange interaction does not depend on the

dx.doi.org/10.1021/ic202755z | Inorg. Chem. 2012, 51, 3289−3301

Table 5. Selected Experimental Magnetostructural Data for Oxalato-Bridged $Cr^{III}M^{II}$ Heteropolynuclear Complexes (M = Mn, Fe, Co, Ni, and Cu)

entry	complex[a]	M	J^b/cm^{-1}	$R^c/Å$	ref.
1	**1**	Co	+2.2	5.423	this work
2	**2**	Mn	+1.2	5.389	this work
3	$[Cr(salen)(ox)Cu(acpy)]\cdot 1.5H_2O$	Cu	+5.6	5.482	15
4	$[Cr(salen)(ox)Ni(taea)]BPh_4\cdot MeOH$	Ni	+9.2	n.a.	15
5	$[Cr(salen)(ox)Co(taea)]BPh_4\cdot MeOH$	Co	+2.6	n.a.	15
6	$[Cr(salen)(ox)Fe(taea)]BPh_4\cdot MeOH$	Fe	+1.6	n.a.	15
7	$[Cr(salen)(ox)Mn(taea)]BPh_4$	Mn	+1.0	n.a.	15
8	$[Cr(bpy)(ox)_2Cu(bpca)(H_2O)]\cdot 2.5H_2O$	Cu	<1.0	5.283[d]	18a
9	$[Cr(phen)(ox)_2Cu(bpca)(H_2O)]\cdot 2H_2O$	Cu	<1.0	5.407[d]	18a
10	$[Cr(bpy)(ox)_2Cu(Hfsaaep)(H_2O)]\cdot 2H_2O$	Cu	+1.4	5.506	18b
11	$[Cr(phen)(ox)_2Mn(phen)_2(N_3)]\cdot H_2O$	Mn	−1.9	5.257[d]	18b
12	$\{[Cr(bpy)(ox)_2]_2Co(H_2O)_2\}\cdot H_2O$	Co	n.a.	5.288	19a
13	$\{[Cr(bpy)(ox)_2]_2Cu(H_2O)_2\}\cdot 1.5H_2O$	Cu	−18.8	5.288	19b
14	$\{[Cr(bpy)(ox)_2]_2Ni(H_2O)_2\}\cdot H_2O$	Ni	−0.6	n.a.	19c
15	$\{[Cr(bpy)(ox)_2]_2Co(Me_2bpy)\}\cdot 2H_2O$	Co	+2.4	n.a.	21a
16	$\{[Cr(phen)(ox)_2]_2Co(Me_2bpy)\}\cdot 1.5H_2O$	Co	+2.3	5.352	21a
17	$\{[Cr(bpy)(ox)_2]_2Co(Me_2phen)\}$	Co	+1.8	n.a.	21b
18	$\{[Cr(phen)(ox)_2Mn(bpy)(H_2O)]_2(ox)\}\cdot 1.5H_2O$	Mn	−1.1	5.504[d]	20a
19	$\{[Cr(bpy)(ox)_2Cu(bpy)]_2(ox)\}\cdot 2H_2O$	Cu	−1.3	5.447	20b
20	$(TTF)_4\{[Cr(ox)_3]_2Cu(H_2O)_2\}\cdot 3H_2O$	Cu	−0.7	n.a.	11b
21	$(TTF)_4\{[Cr(ox)_3]_2Ni(H_2O)_2\}\cdot 6H_2O$	Ni	+6.8	n.a.	11b
22	$(TTF)_4\{[Cr(ox)_3]_2Co(H_2O)_2\}\cdot 8H_2O$	Co	n.a.	n.a.	11b
23	$(TTF)_4\{[Cr(ox)_3]_2Fe(H_2O)_2\}\cdot 4H_2O$	Fe	+1.2	n.a.	11b
24	$(TTF)_4\{[Cr(ox)_3]_2Mn(H_2O)_2\}\cdot 14H_2O$	Mn	+1.1	5.492	11a,b
25	$(Hampy)_4\{[Cr(ox)_3]_2Co(H_2O)_2\}\cdot 3H_2O$	Co	+2.7	5.429	11c
26	$(Hampy)_4\{[Cr(ox)_3]_2Mn(H_2O)_2\}\cdot 3H_2O$	Mn	+1.2	5.510	11c
27	$\{Cr(ox)_3[Ni(Me_6\text{-}[14]ane\text{-}N_4)]_3\}(ClO_4)_3$	Ni	+5.3	n.a.	16a

[a]Abreviations: ox^{2-} = oxalate; bpy = 2,2′-bipyridine; phen = 1,10-phenanthroline; Me_2bpy = 6,6′-dimethyl-2,2′-bipyridine; Me_2phen = 2,9-dimethyl-1,10-phenanthroline; H_2salen = *N*,*N*′-ethylenebis(salicylideneimine); Hacpy = *N*-acetylacetonylidene-*N*-(2-pyridylethyl)amine; taea = tris(2-aminoethyl)amine; BPh_4^- = tetraphenylborate anion; $bpca^-$ = bis(2-pyridylcarbonyl)amidate; H_2fsaaep = 3-[*N*-2-(pyridylethyl)formimidoyl]salicylic acid; $Hampy^+$ = 4-aminopyridinium cation; TTF^+ = tetrathiofulvalene cation; Me_6-[14]ane-N_4 = *rac*-5,7,7,12,14,14-hexamethyl-1,4,8,11-tetraazacyclotetradecane. [b]Intramolecular magnetic coupling parameter ($\mathbf{H} = -J\mathbf{S_{Cr}}\cdot\mathbf{S_M}$). [c]Average intermetallic distance. [d]Bridging bidentate/monodentate (outer) oxalate.

nature of the high-spin M^{II} ion (M = Co and Mn) but on the distinct coordination bridging mode of the oxalato group, either bis(bidentate) ($J > 0$) or bidentate/monodentate (outer) ($J < 0$), respectively. On the other hand, the relative magnitude of the intramolecular ferromagnetic coupling between the Cr^{III} ion and the high-spin M^{II} ion decreases from **1** to **2** [J = +2.2 (M = Co) and +1.2 cm^{-1} (M = Mn); Table 5, entries 1 and 2]. This same trend was previously found in related ferromagnetically coupled, oxalato-bridged chromium(III)-cobalt(II) and chromium(III)-manganese(II) di- and trinuclear complexes of general formula $[Cr(salen)(ox)M(taea)]BPh_4\cdot MeOH$ [J = +2.6 (M = Co) and +1.0 cm^{-1} (M = Mn); Table 5, entries 5 and 7] and $(Hampy)_4\{[Cr(ox)_3]_2M(H_2O)_2\}\cdot 3H_2O$ [J = +2.7 (M = Co) and +1.2 cm^{-1} (M = Mn); Table 5, entries 25 and 26], respectively.[15,11c]

As a matter of fact, the intramolecular magnetic coupling parameter (J) for metal ions with more than one unpaired electron can be decomposed into a sum of individual contributions (J_{ij}) involving each pair of magnetic orbitals (ϕ_i and ϕ_j) according to $J = 1/(n_An_B)\sum_{i,j} J_{ij}$ ($i = 1-n_A$ and $j = 1-n_B$), where n_A and n_B are the number of unpaired electrons on each metal center.[43] Hence, the variation in the overall magnetic coupling is not properly described by J but by the product n_An_BJ through the well-known expression $n_An_BJ = \sum_{i,j} J_{ij}$ ($i = 1-n_A$ and $j = 1-n_B$). That being so, the nature and magnitude of the overall magnetic coupling in the AB pair ultimately depend on several pairwise contributions, which can be either ferro- ($J_{ij} > 0$) or antiferromagnetic ($J_{ij} < 0$) for an orthogonal or nonorthogonal pair of magnetic orbitals with a zero ($S = \langle\phi_i|\phi_j\rangle = 0$) or nonzero ($S = \langle\phi_i|\phi_j\rangle \neq 0$) orbital overlap, respectively.[43] In **1** and **2**, the $3d^3$ Cr^{III} ion possesses a trigonally distorted octahedral geometry with a $(d_{x^2-y^2})^1(d_{xz})^1(d_{yz})^1(d_{xy})^0(d_{z^2})^0$ electronic configuration, whereby the three unpaired electrons occupy the $d_{x^2-y^2}$, d_{xz}, and d_{yz} magnetic orbitals resulting from the splitting of the $t_{2g}(d_{xz}, d_{yz}, d_{x^2-y^2})$ level because of the combined effect of the trigonal twist and trigonal compression. The high-spin $3d^5$ Mn^{II} ion in **2** has a similar trigonally distorted octahedral geometry with a $(d_{x^2-y^2})^1(d_{xz})^1(d_{yz})^1(d_{xy})^1(d_{z^2})^1$ electronic configuration, whereby the two additional unpaired electrons occupy the d_{xy} and d_{z^2} magnetic orbitals resulting from the splitting of the $e_g(d_{z^2}, d_{xy})$ level. In contrast, the high-spin $3d^7$ Co^{II} ion in **1** has a rhombically distorted octahedral geometry with a $(d_{x^2-y^2})^2(d_{xz})^2(d_{yz})^1(d_{xy})^1(d_{z^2})^1$ electronic configuration, the three unpaired electrons occupying the d_{yz}, d_{xy}, and d_{z^2} magnetic orbitals resulting from the splitting of the $t_{2g}(d_{xz}, d_{yz}, d_{x^2-y^2})$ and $e_g(d_{z^2}, d_{xy})$ levels because of the combined effect of axial compression and equatorial bending. This situation gives rise to $n_An_B = 3 \times 3 = 9$ and $n_An_B = 3 \times 5 = 15$ individual magnetic coupling contributions for the oxalato-bridged

dx.doi.org/10.1021/ic202755z | Inorg. Chem. 2012, 51, 3289−3301

Scheme 1. Projection Views of the Pairs of σ- and/or π-Type Magnetic Orbitals of the Cr^{III} (Green) and High-Spin M^{II} Ions (Purple) for the Oxalato-Bridged $Cr^{III}M^{II}$ Dinuclear Entities of 1 (M = Co) and 2 (M = Mn)

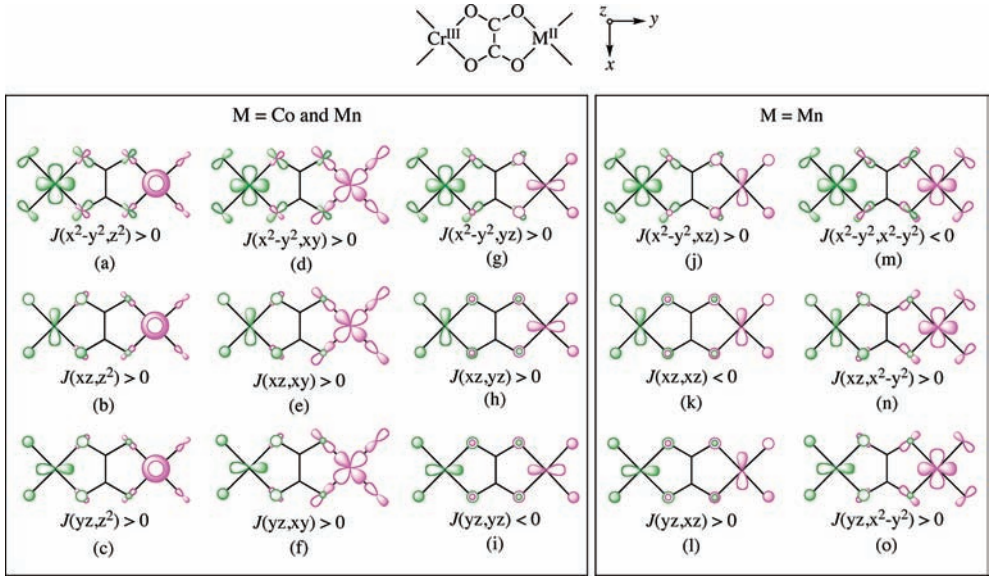

$Cr^{III}M^{II}$ dinuclear entities in **1** (M = Co) and **2** (M = Mn), respectively. They would involve both mixed σ/π-type and purely σ- or π-type orbital pathways as illustrated in Scheme 1, whereby each pair of magnetic orbitals are made up by the singly occupied 3d metal orbitals of the Cr^{III} and high-spin M^{II} ions (M = Co and Mn) mixed with the corresponding σ- or π-type antibonding orbitals of the oxalato bridging ligand of appropriate symmetry.

Hence, the overall ferromagnetic coupling observed in the oxalato-bridged $Cr^{III}M^{II}$ dinuclear entities of **1** (M = Co) and **2** (M = Mn) would be explained by the larger number of positive ferromagnetic contributions. They mainly involve the $d_{x^2-y^2}(Cr)/d_{xy}(M)$, $d_{xz}(Cr)/d_{xy}(M)$, $d_{yz}(Cr)/d_{xy}(M)$, and $d_{xz}(Cr)/d_{yz}(M)$ (M = Co and Mn) as well as $d_{yz}(Cr)/d_{xz}(M)$ (M = Mn) pairs of orthogonal magnetic orbitals which possess a large spin delocalization onto the oxalato bridge with a zero orbital overlap ($S = \langle\phi_i|\phi_j\rangle = 0$ with $i \neq j$, Schemes 1d, e, f, h, and l). As is usually the case for extended bridging ligands like oxalate, they would dominate over the negative antiferromagnetic ones involving exclussively the $d_{yz}(Cr)/d_{yz}(M)$ (M = Co and Mn), $d_{xz}(Cr)/d_{xz}(M)$ (M = Mn), and $d_{x^2-y^2}(Cr)/d_{x^2-y^2}(M)$ (M = Mn) pairs of nonorthogonal magnetic orbitals which also possess a large spin delocalization onto the oxalato bridge with a nonzero orbital overlap ($S = \langle\phi_i|\phi_j\rangle \neq 0$ with $i = j$, Schemes 1i, k, and m). The variation of the overall ferromagnetic coupling for **1** and **2** according to $n_A n_B J = 9J = +19.44\ cm^{-1}$ (**1**) > $n_A n_B J = 15J = +18.30\ cm^{-1}$ (**2**), would be then explained by the increase of the number of individual antiferromagnetic contributions when going from M = Co ($J_{yz,yz} < 0$) to M = Mn ($J_{yz,yz}$, $J_{xz,xz}$, and $J_{x^2-y^2,x^2-y^2} < 0$) and/or the decrease of the magnitude of the ferromagnetic ones ($J_{x^2-y^2,xy}$, $J_{xz,xy}$, $J_{yz,xy}$, $J_{xz,yz}$, and $J_{yz,xz} > 0$) because of the lesser diffuseness of the 3d metal orbitals.

Theoretical Calculations. Several computational methodologies based on the DF theory were used to evaluate the magnetic coupling parameter (J) in the actual structures of **1** and **2** (see Computational Details). Within the framework of the BS approach, the values of the magnetic coupling parameter for the $Cr^{III}M^{II}$ dinuclear entities of **1** (M = Co) and **2** (M = Mn) can be calculated from the energy difference between the spin configurations of lowest BS and highest multiplicity [$\Delta E = E(S = 0) - E(S = 3) = 6J$ (**1**) and $\Delta E = E(S = 1) - E(S = 4) = 9J$ (**2**)], which correspond to the antiparallel (antiferromagnetic) and parallel (ferromagnetic) spin alignment respectively, of the local spin moments of the Cr^{III} ($S_{Cr} = 3/2$) and M^{II} ions [$S_M = 3/2$ (M = Co) and 5/2 (M = Mn)]. The calculated J values for the oxalato-bridged $Cr^{III}M^{II}$ dinuclear entities of **1** (M = Co) and **2** (M = Mn) are listed in Table 6.

Table 6. Experimental and Calculated J Values (cm^{-1}) for the Oxalato-Bridged $Cr^{III}M^{II}$ Dinuclear Entities of 1 (M = Co) and 2 (M = Mn)[a]

method	1	2
B3LYP-BS (gas)	+3.9	−0.3
B3LYP-BS (CH_3CN)	+5.2	+0.4
B3LYP-BS (CH_2Cl_2)	+5.0	+0.8
SIESTA (solid)	+3.9	+12.5
Exp.	+2.2	+1.2

[a]The calculated values of the magnetic coupling parameter (J) have been evaluated from the energy difference between the singlet and septet spin functions for **1** [$\Delta E = E(S = 0) - E(S = 3) = 6J$] and that between the triplet and nonet spin functions for **2** [$\Delta E = E(S = 1) - E(S = 4) = 9J$].

DF energy calculations using the B3LYP hybrid functional on the oxalato-bridged $Cr^{III}M^{II}$ dinuclear entities in the gas phase support the ferromagnetic coupling experimentally found in **1** (M = Co), but they fail to reproduce that found in **2** (M = Mn). This same situation was previously found by Pardo et al. in an attempt to explain the ferromagnetic coupling experimentally observed in a related series of oxalato-bridged $Cr^{III}_2M^{II}$ trinuclear complexes (M = Co and Mn).[11c] Our calculations indicate a ground septet ($S = 3$) spin state that is rather well separated from the excited singlet ($S = 0$) spin state in **1** [$\Delta E = E(S = 0) - E(S = 3) = 6J = +23.4\ cm^{-1}$]. Alternatively, a ground triplet ($S = 1$) spin state is observed in **2** that is very close to the excited nonet ($S = 4$) spin state

dx.doi.org/10.1021/ic202755z | Inorg. Chem. 2012, 51, 3289−3301

[$\Delta E = E(S = 1) - E(S = 4) = 9J = -2.7$ cm^{-1}]. The calculated J value for **1** ($J = +3.9$ cm^{-1}) is in fairly good agreement with the experimental one ($J = +2.2$ cm^{-1}), in terms of both sign and magnitude. This is not the case for **2**, where the calculated J value ($J = -0.3$ cm^{-1}) clearly differs in sign from the experimental one ($J = +1.2$ cm^{-1}).

B3LYP-BS calculations based on the DF theory have been very useful in the evaluation of the magnetic coupling parameters in polynuclear complexes, independently of their sign and even when their values are small. Yet it has been earlier observed that the presence of charged peripheral ligands sharing their charge in a spatial region near to the metal ions can lead to subtle modifications on the electronic structure of the polymetallic species, which ultimately cause important shifts of the magnitude and even of the nature of the magnetic interaction.[44] Clearly, placing opposite charges in close regions is not a suitable or stable situation from an electronic viewpoint, and sometimes partial charge transfers can occur to minimize these electronic effects leading to unexpected predictions which do not agree with the experimental results. In such cases, the inclusion of electronic effects from the solvent or from neighboring molecules in the calculations favors the localization of the excess of charge in the peripheral ligand leading to the electronic stabilization of the system.

In a first approximation, a solvent cavity was used to simulate the variety of hydrogen bonding, van der Waals, and electrostatic interactions between the oxalato-bridged $Cr^{III}M^{II}$ dinuclear cations of **1** (M = Co) and **2** (M = Mn) and the neighboring Cr^{III} mononuclear anions and neutral water molecules that are present in the solid state. Solvation effects were then introduced by using a polarizable continuum model (PCM)[33] with parameters corresponding to the acetonitrile solvent because it often provides us with values of the magnetic coupling parameters of the same order of magnitude as the experimental ones, as earlier checked on several simple complexes. In this model, the solvent cavity is created via a series of overlaping spheres to appropiately calibrate the electronic delocalization effects onto the oxalato bridging ligand that result from the charged nature of the terminal oxalato ligands. When considering the presence of solvent molecules in the B3LYP-BS calculations on **1** and **2** through a PCM approximation, the nature of the magnetic coupling for the oxalato-bridged $Cr^{III}M^{II}$ dinuclear entities (M = Co and Mn) is conveniently modified to be consistent with experience. So, the calculated J values in acetonitrile solution [$J = +5.2$ (**1**) and $+0.4$ cm^{-1} (**2**)] agree both in sign and in magnitude with the experimental ones [$J = +2.2$ (**1**) and $+1.2$ cm^{-1} (**2**)]. Similar results were obtained with other solvents like dichloromethane [$J = +5.0$ (**1**) and $+0.8$ cm^{-1} (**2**)].

Finally, DF periodic calculations in the solid state were carried out to take into account the intermolecular electronic effects due to the presence of the Cr^{III} mononuclear anions that are in close contact with the oxalato-bridged $Cr^{III}M^{II}$ dinuclear cations of **1** (M = Co) and **2** (M = Mn). In this regard, SIESTA is a low time-consuming package program that is particularly useful and efficient for performing such periodic calculations on solids with large crystal cells. The results of the DF periodic calculations in the solid state for **1** using the SIESTA program[35] are comparable to the more accurate B3LYP-BS ones in solution. Although the ferromagnetic nature of the exchange interaction for **2** is preserved, they lead, however, to a significant increase in the magnitude of the magnetic coupling. So, the calculated J value for **1** ($J = +3.9$ cm^{-1}) is close to the experimental one ($J = +2.2$ cm^{-1}) but that for **2** ($J = +12.5$ cm^{-1}) differs by 1 order of magnitude ($J = +1.2$ cm^{-1}). The large dependence of our results on the computational methodology used for the evaluation of the J values in **1** and **2** can be explained from the electronic nature of the metal ions and the large number of orbital pathways, as discussed above. These features determine the inherent difficulty to calibrate properly the electronic delocalization effects onto the oxalato bridge which are ultimately responsible for the overall magnetic coupling.

The NBO analysis[34] of the spin densities for **1** and **2** clearly indicates that the spin delocalization effects through the σ bonds are dominant over the spin polarization effects through the π bonds of the oxalato bridge, as illustrated by the calculated spin density distribution for the septet (**1**) and nonet (**2**) ground spin states in acetonitrile solution (Figure 5). This

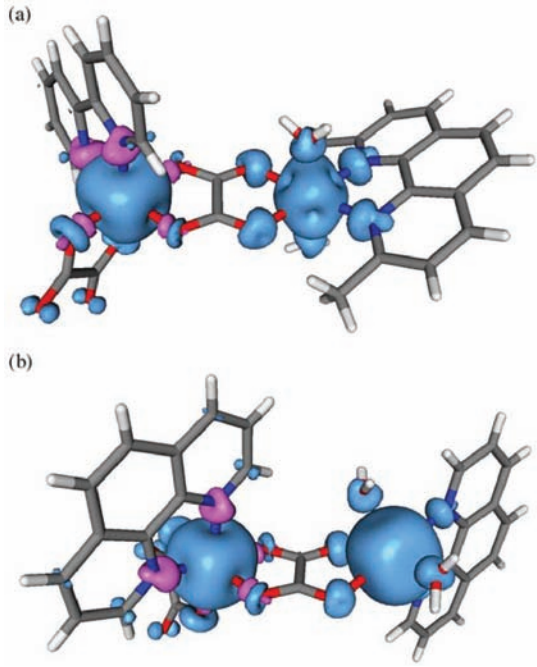

Figure 5. Perspective views of the calculated spin density distribution for the septet and nonet ground spin state configuration of the oxalato-bridged $Cr^{III}M^{II}$ entities of **1** (M = Co) (a) and **2** (M = Mn) (b) respectively, in acetonitrile solution. Blue and violet contours represent positive and negative spin densities, respectively. The isodensity surface corresponds to a cutoff value of 0.0025 e bohr^{-3}.

situation nicely agrees with the σ- and/or π-type nature of the aforementioned pairs of magnetic orbitals of the Cr^{III} and high-spin M^{II} ions in the oxalato-bridged $Cr^{III}M^{II}$ entities (M = Co and Mn) (see Scheme 1). So, the calculated values of the atomic spin density (ρ_X) for the septet (**1**) and nonet (**2**) ground spin states in acetonitrile solution provide a detailed picture of the relative importance of the spin delocalization and spin polarization effects (Table 7). The spin density values for the chromium atom in **1** ($\rho_{Cr} = +2.977$) and **2** ($\rho_{Cr} = +2.980$) are close to that expected for a free $3d^3$ Cr^{III} ion with three unpaired electrons ($n_A = 3$). This agrees with a small spin delocalization from the metal toward the coordinated ligands because of the mainly nonbonding nature of the d_{xz}, d_{yz}, and $d_{x^2-y^2}$ magnetic orbitals of the trigonally distorted octahedral Cr^{III} ion. In contrast, the spin density values for the cobalt and manganese atoms in **1** ($\rho_{Co} = +2.766$) and **2** ($\rho_{Mn} = +4.827$)

dx.doi.org/10.1021/ic202755z | Inorg. Chem. 2012, 51, 3289–3301

Table 7. Calculated Values of the Atomic Spin Densities (e) for the Septet and Nonet Ground Spin State Configurations of the Oxalato-Bridged $Cr^{III}M^{II}$ Entities of 1 (M = Co) and 2 (M = Mn), Respectively[a,b]

	1	2
Cr(1)	+2.977	+2.980
N(3)	−0.047	−0.045
N(4)	−0.043	−0.047
O(3)	−0.013	−0.008
O(4)	−0.010	−0.007
O(5)	−0.003	+0.002
O(6)	−0.001	−0.005
C(1)	+0.007	+0.010
C(2)	+0.006	+0.014
M(1)	+2.766	+4.827
N(1)	+0.052	+0.019
N(2)	+0.055	+0.018
O(1)	+0.043	+0.026
O(2)	+0.044	+0.029
O(1w)	+0.036	+0.023
O(2w)	+0.028	+0.019
C(1)	+0.007	+0.010
C(2)	+0.006	+0.014

[a]The calculated values of the atomic spin densities (ρ_X) have been determined in acetonitrile solution using the DF (B3LYP-BS) method. [b]The atom-numbering schemes for **1** and **2** are given in Figures 1a and 1b, respectively.

are smaller than those expected for a free high-spin $3d^7$ Co^{II} and $3d^5$ Mn^{II} ions with three (n_B = 3) and five unpaired electrons (n_B = 5), respectively. This feature reflects a significant spin delocalization from the metal toward the coordinated ligands because of the strong ligand participation in the antibonding d_{z^2} and d_{xy} magnetic orbitals of the rhombically or trigonally distorted octahedral M^{II} ions (M = Co and Mn, respectively).

On the other hand, the spin density values for the imine-nitrogen (ρ_N in the range of −0.043 to −0.047) and carboxylate-oxygen (ρ_O in the range of +0.043 to −0.013) donor atoms directly coordinated to the Cr^{III} ion have an overall negative sign in **1** and **2**. These spin polarization effects are likely explained by the partial electron donation from the donor atoms of the coordinated ligands toward the empty d_{z^2} and d_{xy} magnetic orbitals of the octahedral Cr^{III} ion. The M^{II} ions in **1** (M = Co) and **2** (M = Mn) show instead positive values of the spin density for the imine-nitrogen [ρ_N = +0.052 and +0.055 (**1**), or +0.018 and +0.019 (**2**)] and the carboxylate- [ρ_O = +0.043 and +0.044 (**1**), or +0.026 and +0.029 (**2**)] and aqua-oxygen atoms [ρ_{Ow} = +0.028 and +0.036 (**1**), or +0.019 and +0.023 (**2**)]. Moreover, they show an overall decrease on going from **1** to **2**, as expected from the different diffuseness of the 3d orbitals for each M^{II} ion (M = Co and Mn). Interestingly, the calculated values of the spin density for the central carbon atoms of the oxalato bridge are very small but nonnegligible, and they have a positive sign [ρ_C = +0.006 and +0.007 (**1**), or +0.010 and +0.014 (**2**)], indicating that the spin delocalization effects dominates over the spin polarization ones.

CONCLUSION

In this work, we show that novel oxalato-bridged chromium(III)-cobalt(II) (**1**) and chromium(III)-manganese(II) (**2**) dinuclear complexes can be obtained from bis(oxalato)-chromate(III) mononuclear complexes acting as both discrete anions and bidentate metalloligands toward hydrated cobalt(II) and manganese(II) mononuclear complexes with aromatic α,α'-diimine and their β,β'-dimethyl-substituted derivatives as blocking ligands. The packing of the anionic mononuclear and cationic heterodinuclear complexes through hydrogen bonding interactions between the free carbonyl groups from oxalate (hydrogen acceptors) and the two *trans* (**1**) or *cis* (**2**) coordinated water molecules (hydrogen donors) leads to hydrogen-bonded chains with either ladder- (**1**) or ribbon-like (**2**) architectures in the solid state.

This new type of homo- and heteroleptic oxalato-bridged $Cr^{III}M^{II}$ heterodinuclear complexes (M = Co and Mn) with identical or different aromatic diimine ligands respectively, exhibit a weak intramolecular ferromagnetic coupling between the Cr^{III} and high-spin M^{II} ions (M = Co and Mn) across the oxalato bridge to give S = 3 $Cr^{III}Co^{II}$ (**1**) and S = 4 $Cr^{III}Mn^{II}$ (**2**) ground spin states, as supported by DF electronic structure calculations. However, it should be emphasized that the approximations made in the theoretical calculations are such that a perfect agreement with experience cannot be found in that case. In fact, this is a very difficult task because of the large number of individual contributions, both ferro- and antiferromagnetic, which would be much larger than the small (close to zero) values of the magnetic coupling parameter for **1** and **2**. So, the resultant ferromagnetic nature of the electron exchange interaction between the Cr^{III} ion and the high-spin M^{II} ions within the oxalato-bridged $Cr^{III}M^{II}$ entities (M = Co and Mn) involves a subtle competition between σ- and/or π-orbital pathways possessing a significant spin delocalization and only a small but non-negligible sign alternation of the spin densities within the oxalato bridge, indicating thus that the spin delocalization mechanism dominates over the spin polarization one.

ASSOCIATED CONTENT

Supporting Information

Crystallographic data in CIF format. This material is available free of charge via the Internet at http://pubs.acs.org. Crystallographic data (excluding structure factors) for **1** and **2** have been deposited with the Cambridge Crystallographic Data Centre as supplementary publication numbers CCDC−650176 (**1**) and CCDC−845146 (**2**). Copies of the data can be obtained free of charge on application to CCDC, 12 Union Road, Cambridge CB21EZ, U.K. (fax: (+44) 1223 336 033; e-mail: deposit@ccdc.cam.ac.uk).

AUTHOR INFORMATION

Corresponding Author

*E-mail: isabel.castro@uv.es (I.C.), joan.cano@uv.es (J.C.)

Notes

The authors declare no competing financial interest.

ACKNOWLEDGMENTS

This work was supported by the MICINN (Spain) (Projects CTQ2010-15364, MAT2010-16981, CSD2007-00010, CSD2006-00015, and DPI2010-21103-C04-03), the Generalitat Valenciana (Spain) (Project PROMETEO/2009/108), and the ACIISI-Gobierno Autónomo de Canarias (Spain) (Project PIL-2070901). We are specially indebted to Jesús Ferrando-Soria for his assistance in the magnetic measurements.

REFERENCES

(1) (a) Kahn, O. *Struct. Bonding (Berlin)* **1987**, *68*, 89. (b) Kahn, O. *Adv. Inorg. Chem.* **1995**, *43*, 179. (c) Pilkington, M.; Gross, M.; Franz, P.; Biner, M.; Decurtins, S.; Stoeckli-Evans, H.; Neels, A. *J. Solid State Chem.* **2001**, *159*, 262. (d) Linert, W.; Verdaguer, M. *Molecular Magnets. Recent Highlights*; Springer Verlag: Berlin, Germany, 2003. (e) Pilkington, M.; Decurtins, S. In *Comprehensive Coordination Chemistry II: From Biology to Nanotechnology*; McCleverty, J. A., Meyer, T. J., Eds.; Elsevier Pergamon: Amsterdam, The Netherlands, 2004; Vol. 7, p 177. (f) Dechambenoit, P.; Long, J. R. *Chem. Soc. Rev.* **2011**, *40*, 3249. (g) Miller, J. S. *Chem. Soc. Rev.* **2011**, *40*, 3266. (h) Train, C.; Gruselle, M.; Verdaguer, M. *Chem. Soc. Rev.* **2011**, *40*, 3297.

(2) (a) Verdaguer, M.; Bleuzen, A.; Marvaud, V.; Vaissermann, J.; Seuleiman, M.; Desplanches, C.; Scuiller, A.; Train, C.; Garde, R.; Gelly, G.; Lomenech, C.; Rosenman, I.; Veillet, P.; Cartier, C.; Villain, F. *Coord. Chem. Rev.* **1999**, *190*−*192*, 1023. (b) Ohba, M.; Okawa, H. *Coord. Chem. Rev.* **2000**, *198*, 313. (c) Lescouëzec, R.; Toma, L. M.; Vaissermann, J.; Verdaguer, M.; Delgado, F. S.; Ruiz-Pérez, C.; Lloret, F.; Julve, M. *Coord. Chem. Rev.* **2005**, *249*, 2691.

(3) (a) Decurtins, S.; Pellaux, R.; Antorrena, G.; Palacio, F. *Coord. Chem. Rev.* **1999**, *190*−*192*, 841. (b) Coronado, E.; Clemente-León, M.; Galán-Mascarós, J. R.; Giménez-Saiz, C.; Gómez-García, C. J.; Martínez-Ferrero, E. *J. Chem. Soc., Dalton Trans.* **2000**, 3955. (c) Coronado, E.; Forment-Aliaga, A.; Galán-Mascarós, J. R.; Giménez-Saiz, C.; Gómez-García, C. J.; Martínez-Ferrero, E.; Nuez, A.; Romero, F. M. *Solid State Sci.* **2003**, *5*, 917. (d) Coronado, E.; Galán-Mascarós, J. R. *J. Mater. Chem.* **2005**, *15*, 66. (e) Gruselle, M.; Train, C.; Boubekeur, K.; Gredin, P.; Ovanesyan, N. *Coord. Chem. Rev.* **2006**, *250*, 2491.

(4) (a) Kahn, O. *Struct. Bonding (Berlin)* **1987**, *68*, 89. (b) Journaux, Y.; Ruiz, R.; Aukauloo, A.; Pei, Y. *Mol. Cryst. Liq. Cryst.* **1997**, *305*, 193. (c) Ruiz, R.; Faus, J.; Lloret, F.; Julve, M.; Journaux, Y. *Coord. Chem. Rev.* **1999**, *193*−*195*, 1069. (d) Kahn, O. *Acc. Chem. Res.* **2000**, *33*, 647. (e) Pardo, E.; Ruiz-García, R.; Cano, J.; Ottenwaelder, X.; Lescouëzec, R.; Journaux, Y.; Lloret, F.; Julve, M. *Dalton Trans.* **2008**, 2780. (f) Dul, M.-C.; Pardo, E.; Lescouëzec, R.; Journaux, Y.; Ferrando-Soria, J.; Ruiz-García, R.; Cano, J.; Julve, M.; Lloret, F.; Cangussu, D.; Pereira, C. L. M.; Stumpf, H. O.; Pasán, J.; Ruiz-Pérez, C. *Coord. Chem. Rev.* **2010**, *254*, 2281.

(5) (a) Ohkoshi, S.-I.; Arai, K.-I.; Sato, Y.; Hashimoto, K. *Nat. Mater.* **2003**, *2*, 857. (b) Yanai, N.; Kaneko, W.; Yoneda, K.; Ohba, M.; Kitagawa, S. *J. Am. Chem. Soc.* **2007**, *129*, 3496. (c) Kaneko, W.; Ohba, M.; Kitagawa, S. *J. Am. Chem. Soc.* **2007**, *129*, 13706. (d) Milon, J.; Daniel, M.-C.; Kaiba, A.; Guionneau, P.; Brandès, S.; Sutter, J.-P. *J. Am. Chem. Soc.* **2007**, *129*, 13872. (e) Kaye, S. S.; Choi, H. J.; Long, J. R. *J. Am. Chem. Soc.* **2008**, *130*, 16921. (f) Pinkowicz, D.; Podgajny, R.; Balanda, M.; Makarewicz, M.; Gawel, B.; Lasocha, W.; Sieklucka, B. *Inorg. Chem.* **2008**, *47*, 9745.

(6) (a) Inoue, K.; Kikuchi, K.; Ohba, M.; Okawa, H. *Angew. Chem., Int. Ed.* **2003**, *42*, 4810. (b) Train, C.; Gheorge, R.; Krstic, V.; Chamoreau, L.-M.; Ovanesyan, N. S.; Rikken, G. L. J. A.; Gruselle, M.; Verdaguer, M. *Nat. Mater.* **2008**, *7*, 729. (c) Train, C.; Nuida, T.; Gheorge, R.; Gruselle, M.; Ohkoshi, S. *J. Am. Chem. Soc.* **2009**, *131*, 16838.

(7) (a) Clemente-León, M.; Coronado, E.; López-Jordá, M. *Dalton Trans.* **2010**, *39*, 4903. (b) Clemente-León, M.; Coronado, E.; López-Jordá, M.; Waerenborgh, J. C. *Inorg. Chem.* **2011**, *50*, 9122.

(8) (a) Sato, O.; Iyoda, T.; Fujishima, A.; Hashimoto, K. *Science* **1996**, *272*, 704. (b) Bleuzen, A.; Lomenech, C.; Escax, V.; Villain, F.; Varret, F.; Cartier, C.; Verdaguer, M. *J. Am. Chem. Soc.* **2000**, *122*, 6648. (c) Bénard, S.; Riviére, E.; Yu, P.; Nakatani, K.; Delouis, J. F. *Chem. Mater.* **2001**, *13*, 441. (d) Lacroix, P. G.; Malfant, I.; Bénard, S.; Yu, P.; Riviére, E.; Nakatani, K. *Chem. Mater.* **2001**, *13*, 441. (e) Bénard, S.; Yu, P.; Audiére, J. P.; Riviére, E.; Clèment, R.; Ghilhelm, J.; Tchertanov, L.; Nakatani, K. *J. Am. Chem. Soc.* **2000**, *122*, 9444. (f) Cariati, E.; Macchi, R.; Roberto, D.; Ugo, R.; Galli, S.; Casati, N.; Macchi, P.; Sironi, A.; Bogani, L.; Caneschi, A.; Gatteschi, D. *J. Am. Chem. Soc.* **2000**, *129*, 9410. (g) Coronado, E.; Giménez-López, M. C.; Korzeniak, T.; Levchenko, G.; Romero, F. M.; Segura, A.; García-Baonza, V.; Cezar, J. C.; De Groot, F. M. F.; Milner, A.; Paz-Pasternak, M. *J. Am. Chem. Soc.* **2008**, *130*, 15519.

(9) Ohkoshi, S.; Tokoro, H.; Matsuda, T.; Takahashi, H.; Irie, H.; Hashimoto, K. *Angew. Chem., Int. Ed.* **2007**, *46*, 3238.

(10) (a) Coronado, E.; Galán-Mascarós, J. R.; Gómez-García, C. J.; Laukhin, V. *Nature* **2000**, *408*, 447. (b) Alberola, A.; Coronado, E.; Galán-Mascarós, J. R.; Giménez-Saiz, C.; Gómez-García, C. J. *J. Am. Chem. Soc.* **2003**, *125*, 10774. (c) Pardo, E.; Train, C.; Gontard, G.; Boubekeur, K.; Fabelo, O.; Liu, H.; Dkhil, B.; Lloret, F.; Nakagawa, K.; Tokoro, H.; Ohkoshi, S.; Verdaguer, M. *J. Am. Chem. Soc.* **2011**, *133*, 15328.

(11) (a) Coronado, E.; Galán-Mascarós, J. R.; Giménez-Saiz, C.; Gómez-García, C. J.; Ruiz-Pérez, C.; Triki, S. *Adv. Mater.* **1996**, *8*, 737. (b) Coronado, E.; Galán-Mascarós, J. R.; Giménez-Saiz, C.; Gómez-García, C. J.; Ruiz-Pérez, C. *Eur. J. Inorg. Chem.* **2003**, 2290. (c) Pardo, E.; Train, C.; Lescouëzec, R.; Boubekeur, K.; Ruiz, E.; Lloret, F.; Verdaguer, M. *Dalton Trans.* **2010**, *39*, 4951.

(12) (a) Coronado, E.; Galán-Mascarós, J. R.; Gómez-García, C. J.; Martí-Gastaldo, C. *Inorg. Chem.* **2005**, *44*, 6197. (b) Coronado, E.; Galán-Mascarós, J. R.; Martí-Gastaldo, C. *J. Am. Chem. Soc.* **2008**, *130*, 14987. (c) Coronado, E.; Galán-Mascarós, J. R.; Martí-Gastaldo, C. *CrystEngComm* **2009**, *11*, 2143.

(13) (a) Zhong, Z. J.; Matsumoto, N.; Okawa, H.; Kida, S. *Chem. Lett.* **1990**, 87. (b) Tamaki, H.; Zhong, Z. J.; Matsumoto, N.; Kida, S.; Koikawa, M.; Achiwa, N.; Hashimoto, Y.; Okawa, H. *J. Am. Chem. Soc.* **1992**, *114*, 6974. (c) Okawa, H.; Matsumoto, N.; Tamaki, H.; Ohba, M. *Mol. Cryst. Liq. Cryst.* **1993**, *232*, 617. (d) Clemente-León, M.; Coronado, E.; Galán-Mascarós, J. R.; Gómez-García, C. J. *Chem Commun.* **1997**, 1721. (e) Pellaux, R.; Schmalle, H. W.; Huber, R.; Fischer, P.; Hauss, T.; Ouladdiaf, B.; Decurtins, S. *Inorg. Chem.* **1997**, *36*, 2301. (f) Coronado, E.; Galán-Mascarós, J. R.; Martí-Gastaldo, C. *J. Mater. Chem.* **2006**, *16*, 2685. (g) Coronado, E.; Galán-Mascarós, J. R.; Martí-Gastaldo, C. *Inorg. Chem.* **2006**, *45*, 1882. (h) Coronado, E.; Galán-Mascarós, J. R.; Martí-Gastaldo, C.; Murcia-Martínez, A. *Dalton Trans.* **2006**, 3294. (i) Coronado, E.; Galán-Mascarós, J. R.; Martí-Gastaldo, C. *Inorg. Chem.* **2007**, *46*, 8108. (j) Coronado, E.; Giménez-Saiz, C.; Gómez-García, C. J.; Romero, F. M.; Tarazón, A. *J. Mater. Chem.* **2008**, *18*, 929. (k) Coronado, E.; Martí-Gastaldo, C.; Galán-Mascarós, J. R.; Cavallini, M. *J. Am. Chem. Soc.* **2010**, *132*, 5456.

(14) (a) Decurtins, S.; Schmalle, H. W.; Schneuwly, P.; Ensling, J.; Gütlich, P. *J. Am. Chem. Soc.* **1994**, *116*, 9521. (b) Coronado, E.; Galán-Mascarós, J. R.; Gómez-García, C. J.; Martínez-Agudo, J. M. *Inorg. Chem.* **2001**, *40*, 113. (c) Ballester, G.; Coronado, E.; Giménez-Saiz, C.; Romero, F. M.; Tarazón, A. *Angew. Chem., Int. Ed.* **2001**, *40*, 792. (d) Clemente-León, M.; Coronado, E.; Gómez-García, C. J.; Soriano-Portillo, A. *Inorg. Chem.* **2006**, *45*, 5653.

(15) Ohba, M.; Tamaki, H.; Matsumoto, N.; Okawa, H. *Inorg. Chem.* **1993**, *32*, 5385.

(16) (a) Pei, Y.; Journaux, Y.; Kahn, O. *Inorg. Chem.* **1989**, *28*, 100. (b) Mitsumi, M.; Okawa, H.; Sakiyama, H.; Ohba, M.; Matsumoto, N.; Kurisaki, T.; Wakita, H. *J. Chem. Soc., Dalton Trans.* **1993**, 2991.

(17) Marinescu, G.; Andruh, M.; Lloret, F.; Julve, M. *Coord. Chem. Rev.* **2011**, *255*, 161.

(18) (a) Lescouëzec, R.; Marinescu, G.; Vaissermann, J.; Lloret, F.; Faus, J.; Andruh, M.; Julve, M. *Inorg. Chim. Acta* **2003**, *350*, 131. (b) Marinescu, G.; Visinescu, D.; Cucos, A.; Andruh, M.; Journaux, Y.; Kravtsov, V.; Simonov, Y. A.; Lipkowski, J. *Eur. J. Inorg. Chem.* **2004**, 2914. (c) Nastase, S.; Maxim, C.; Yuna, F.; Duhayon, C.; Sutter, J. P.; Andruh, M. *Polyhedron* **2009**, *28*, 1688.

(19) (a) Rochon, F. D.; Melanson, R.; Andruh, M. *Inorg. Chem.* **1996**, *35*, 6086. (b) Andruh, M.; Melanson, R.; Stager, C. V.; Rochon, F. D. *Inorg. Chim. Acta* **1996**, *251*, 309. (c) Stanica, N.; Stager, C. V.; Cimpoesu, M.; Andruh, M. *Polyhedron* **1998**, *17*, 1787.

(20) (a) Marinescu, G.; Andruh, M.; Lescouëzec, R.; Muñoz, M. C.; Cano, J.; Lloret, F.; Julve, M. *New J. Chem.* **2000**, *24*, 527. (b) Coronado, E.; Giménez, M. C.; Gómez-García, C. J.; Romero, F. M. *Polyhedron* **2003**, *22*, 3115.

(21) (a) Vallejo, J.; Castro, I.; Cañadillas-Delgado, L.; Ruiz-Pérez, C.; Ferrando-Soria, J.; Ruiz-García, R.; Cano, J.; Lloret, F.; Julve, M.

Dalton Trans. **2010**, *39*, 2350. (b) Vallejo, J.; Castro, I.; Ferrando-Soria, J.; Déniz-Hernández, M. P.; Ruiz-Pérez, C.; Lloret, F.; Julve, M.; Ruiz-García, R.; Cano, J. *Inorg. Chem.* **2011**, *50*, 2073.
(22) (a) Martínez-Lillo, J.; Armentano, D.; De Munno, G.; Wernsdorfer, W.; Julve, M.; Lloret, F.; Faus, J. *J. Am. Chem. Soc.* **2006**, *128*, 14218. (b) Martínez-Lillo, J.; Armentano, D.; De Munno, G.; Wernsdorfer, W.; Clemente-Juan, J. M.; Krzystek, J.; Lloret, F.; Julve, M.; Faus, J. *Inorg. Chem.* **2009**, *48*, 3027. (c) Martínez-Lillo, J.; Mastropietro, T. F.; De Munno, G.; Lloret, F.; Julve, M.; Faus, J. *Inorg. Chem.* **2011**, *50*, 5731.
(23) (a) Russell, V.; Craig, D.; Scudder, M.; Dance, I. *CrystEngComm* **2001**, *3*, 96. (b) Muñoz, M. C.; Julve, M.; Lloret, F.; Faus, J.; Andruh, M. *J. Chem. Soc., Dalton Trans.* **1998**, 3125.
(24) (a) Hooft, R. W. W. *COLLECT*; Nonius BV: Delft, The Netherlands, 1999. (b) Duisenberg, A. J. M.; Kroon-Batenburg, L. M. J.; Schreurs, A. M. M. *J. Appl. Crystallogr.* **2003**, *36*, 220 (EVALCCD).
(25) *SADABS*, version 2.03; Bruker AXS Inc.: Madison, WI, 2000.
(26) Sheldrick, G. M. *SHELX97, Programs for Crystal Structure Analysis, release 97-2*; Institüt für Anorganische Chemie der Universität Göttingen: Göttingen, Germany, 1998.
(27) Farrugia, L. J. *J. Appl. Crystallogr.* **1999**, *32*, 837 (*WINGX*).
(28) (a) Nardelli, M. *J. Appl. Crystallogr.* **1995**, *28*, 659. (b) Palmer, D. *CRYSTAL MAKER*; Cambridge University Technical Services: Cambridge, U.K., 1996.
(29) Becke, A. D. *J. Chem. Phys.* **1993**, *98*, 5648.
(30) (a) Ruiz, E.; Cano, J.; Alvarez, S.; Alemany, P. *J. Comput. Chem.* **1999**, *20*, 1391. (b) Ruiz, E.; Rodriguez-Fortea, A.; Cano, J.; Alvarez, S.; Alemany, P. *J. Comput. Chem.* **2003**, *24*, 982.
(31) Frisch, M. J.; Trucks, G. W.; Schlegel, H. B.; Scuseria, G. E.; Robb, M. A.; Cheeseman, J. R.; Scalmani, G.; Barone, V.; Mennucci, B.; Petersson, G. A.; Nakatsuji, H.; Caricato, M.; Li, X.; Hratchian, H. P.; Izmaylov, A. F.; Bloino, J.; Zheng, G.; Sonnenberg, J. L.; Hada, M.; Ehara, M.; Toyota, K.; Fukuda, R.; Hasegawa, J.; Ishida, M.; Nakajima, T.; Honda, Y.; Kitao, O.; Nakai, H.; Vreven, T.; Montgomery, Jr., J. A.; Peralta, J. E.; Ogliaro, F.; Bearpark, M.; Heyd, J. J.; Brothers, E.; Kudin, K. N.; Staroverov, V. N.; Kobayashi, R.; Normand, J.; Raghavachari, K.; Rendell, A.; Burant, J. C.; Iyengar, S. S.; Tomasi, J.; Cossi, M.; Rega, N.; Millam, J. M.; Klene, M.; Knox, J. E.; Cross, J. B.; Bakken, V.; Adamo, C.; Jaramillo, J.; Gomperts, R.; Stratmann, R. E.; Yazyev, O.; Austin, A. J.; Cammi, R.; Pomelli, C.; Ochterski, J. W.; Martin, R. L.; Morokuma, K.; Zakrzewski, V. G.; Voth, G. A.; Salvador, P.; Dannenberg, J. J.; Dapprich, S.; Daniels, A. D.; Farkas, Ö.; Foresman, J. B.; Ortiz, J. V.; Cioslowski, J.; Fox, D. J. *Gaussian 09*, revision A.1; Gaussian, Inc.: Wallingford, CT, 2009.
(32) (a) Schaefer, A.; Horn, H.; Ahlrichs, R. *J. Chem. Phys.* **1992**, *97*, 2571. (b) Schaefer, A.; Huber, C.; Ahlrichs, R. *J. Chem. Phys.* **1994**, *100*, 5829.
(33) (a) Cossi, M.; Rega, N.; Scalmani, G.; Barone, V. *J. Comput. Chem.* **2003**, *24*, 669. (b) Tomasi, J.; Mennucci, B.; Cances, E. *J. Mol. Struct.-Theochem.* **1999**, *464*, 211.
(34) (a) Carpenter, J. E.; Weinhold, F. *J. Mol. Struct.* **1988**, *169*, 41. (b) Reed, A. E.; Curtis, L. A.; Weinhold, F. *Chem. Rev.* **1988**, *88*, 899. (c) Weinhold, F.; Carpenter, J. E. *The Structure of Small Molecules and Ions*; Plenum: New York, 1988; p 227.
(35) Artacho, E.; Gale, J. D.; García, A.; Junquera, J.; Martin, R. M.; Ordejón, P.; Sánchez-Portal, D.; Soler, J. M. *SIESTA* 1.3; 2001.
(36) (a) Perdew, J.; Burke, K.; Ernzerhof, M. *Phys. Rev. Lett.* **1996**, *77*, 3865. (b) Hammer, B.; Hansen, L. B.; Norskov, J. K. *Phys. Rev. B* **1999**, *59*, 7413.
(37) (a) Massobrio, C.; Ruiz, E. *Monatsh. Chem.* **2003**, *134*, 317. (b) Ruiz, E.; Rodríguez-Fortea, A.; Tercero, J.; Cauchy, T.; Massobrio, C. *J. Chem. Phys.* **2005**, *123*, 074102.
(38) Kleinman, L.; Bylander, D. M. *Phys. Rev. Lett.* **1982**, *48*, 1425.
(39) Trouiller, N.; Martins, J. L. *Phys. Rev. B* **1991**, *43*, 1993.
(40) Stiefel, E. I.; Brown, G. F. *Inorg. Chem.* **1972**, *11*, 434.
(41) Lloret, F.; Julve, M.; Cano, J.; Ruiz-García, R.; Pardo, E. *Inorg. Chim. Acta* **2008**, *361*, 3432.
(42) Cano, J. *VPMAG package*; University of Valencia: Valencia, Spain, 2003.
(43) Kahn, O. *Molecular Magnetism*; VCH: New York, 1993.
(44) (a) Visinescu, D.; Toma, L. M.; Cano, J.; Fabelo, O.; Ruiz-Pérez, C.; Labrador, A.; Lloret, F.; Julve, M. *Dalton Trans.* **2010**, *39*, 5028. (b) Nastase, S.; Maxim, C.; Andruh, M.; Cano, J.; Ruiz-Pérez, C.; Faus, J.; Lloret, F.; Julve, M. *Dalton Trans.* **2011**, *40*, 4898. (c) Pardo, E.; Verdaguer, M.; Herson, P.; Rousseliere, H.; Cano, J.; Fabelo, O.; Julve, M.; Lloret, F.; Lescouëzec, R. *Inorg. Chem.* **2011**, *50*, 6250.